Despeckle Filtering Algorithms and Software for Ultrasound Imaging

Despeckle Filtering Algorithms and Software for Ultrasound Imaging
Christos P. Loizou and Constantinos S. Pattichis
www.morganclaypool.com

ISBN: 9781598296204 paperback

ISBN: 9781598296211 ebook

DOI: 10.2200/S00116ED1V01Y200805ASE001

A Publication in the Morgan & Claypool Publishers series

SYNTHESIS LECTURES ON ALGORITHMS AND SOFTWARE IN ENGINEERING #1

Lecture #1

Series Editor: Andreas Spanias, Arizona State University

Series ISSN pending with U.S. Library of Congress

Despeckle Filtering Algorithms and Software for Ultrasound Imaging

Christos P. Loizou
Intercollege, Cyprus

Constantinos S. Pattichis
University of Cyprus

SYNTHESIS LECTURES ON ALGORITHMS AND SOFTWARE IN ENGINEERING #1

MORGAN & CLAYPOOL PUBLISHERS

ABSTRACT

It is well-known that speckle is a multiplicative noise that degrades image quality and the visual evaluation in ultrasound imaging. This necessitates the need for robust despeckling techniques for both routine clinical practice and teleconsultation. The goal for this book is to introduce the theoretical background (equations), the algorithmic steps, and the MATLAB™ code for the following group of despeckle filters: linear filtering, nonlinear filtering, anisotropic diffusion filtering and wavelet filtering. The book proposes a comparative evaluation framework of these despeckle filters based on texture analysis, image quality evaluation metrics, and visual evaluation by medical experts, in the assessment of cardiovascular ultrasound images recorded from the carotid artery. The results of our work presented in this book, suggest that the linear local statistics filter *DsFlsmv*, gave the best performance, followed by the nonlinear geometric filter *DsFgf4d*, and the linear homogeneous mask area filter *DsFlsminsc*. These filters improved the class separation between the asymptomatic and the symptomatic classes (of ultrasound images recorded from the carotid artery for the assessment of stroke) based on the statistics of the extracted texture features, gave only a marginal improvement in the classification success rate, and improved the visual assessment carried out by two medical experts. A despeckle filtering analysis and evaluation framework is proposed for selecting the most appropriate filter or filters for the images under investigation. These filters can be further developed and evaluated at a larger scale and in clinical practice in the automated image and video segmentation, texture analysis, and classification not only for medical ultrasound but for other modalities as well, such as synthetic aperture radar (SAR) images.

KEYWORDS

Speckle, despeckle, noise filtering, ultrasound, ultrasound imaging, cardiovascular imaging, SAR, texture, image quality, carotid artery

Dedication

To my wife, Phaedra; my son, Panayiotis; my daughter, Andrea; and my parents, Panayiotis and Eleni Loizou

Christos P. Loizou

To my family

Constantinos S. Pattichis

"Show thyself in all things an example of good works,
in teaching, in integrity and dignity;
let thy speech be sound and blameless,
so that anyone opposing may be put to shame,
having nothing bad to say for us.
Exhort slaves to obey their masters,
pleasing them in all things and not opposing them."

Titus 2: 7–9

Preface

Speckle is a multiplicative noise that degrades image quality and the visual evaluation in ultrasound and SAR imaging. This necessitates the need for robust despeckling techniques in a wide spectrum of the aforementioned imaging applications. Despeckle filtering applications has been a rapidly emerging research area in recent years. The goal for this book is to introduce the theoretical background (equations), the algorithmic steps, and the MATLAB™ code for the following group of despeckle filters: linear filtering, nonlinear filtering, anisotropic diffusion filtering, and wavelet filtering. The filters covered represent only a snapshot of the vast number of despeckle filters published in the literature. Moreover, selected representative applications of image despeckling covering a variety of ultrasound image processing tasks are presented. Most importantly, a despeckle filtering and evaluation protocol is proposed based on texture analysis, image quality evaluation metrics, and visual evaluation by experts. The source code of the algorithms presented in this book has been made available on the web, thus enabling researchers to more easily exploit the application of despeckle filtering in their problems under investigation.

The book is organized in six chapters. Chapter 1 presents a brief overview of ultrasound imaging, speckle noise, modeling, and filtering. In Chapter 2, the theoretical background (equations), the algorithmic steps, and the MATLAB™ code of selected despeckle filters are presented. Chapter 3 covers the material and recording of ultrasound images, and the evaluation methodology based on texture and statistical analysis, image quality evaluation metrics, and the experiments carried out for visual evaluation. Chapter 4 presents the applications of despeckle filtering techniques in ultrasound images of the carotid and cardiac ultrasound images. Chapter 5 discusses, compares, and evaluates the proposed despeckle filtering techniques where strong and weak points for each filtering technique are presented. Chapter 6 presents the summary and future directions, where a despeckling filtering protocol is also proposed. Finally, at the end of this book, an appendix provides details about the despeckle filtering MATLAB™ toolbox which can also be downloaded at http://www.medinfo.cs.ucy.ac.cy.

This book is intended for all those working in the field of image and video processing technologies, and more specifically in medical imaging and in ultrasound image and video preprocessing and analysis. It provides different levels of material to researchers, biomedical engineers, computing engineers, and medical imaging engineers interested in developing imaging systems with better quality images, limiting the corruption of speckle noise.

Acknowledgments

We thank all the members of our carotid ultrasound imaging team for the long discussions, advice, encouragement, and constructive criticism they provided us during the course of this research work. First of all, we express our sincere thanks to Emeritus Prof. Andrew Nicolaides of the Faculty of Medicine, Imperial College of Science, Technology and Medicine, London, UK, and founder of the Vascular Screening and Diagnostic Centre, Nicosia, Cyprus. Furthermore, we thank Dr. Marios Pantziaris, consultant neurologist at the Cyprus Institute of Neurology & Genetics, Nicosia, Cyprus, Dr. Theodosis Tyllis, consultant physician in the private sector in Cyprus, Associate Professor Efthyvoulos Kyriakou at the Frederick University, Lemesos, Cyprus, Dr. Christodoulos Christodoulou, research associate at the Nicosia, University of Cyprus, and Associate Professor Marios Pattichis, University of New Mexico, Las Cruces, NM. Last but not the least, we would like to thank Prof. Andreas Spanias, Arizona State University, Tempe, AZ, for his proposal and encouragement in writing this book and Joel Claypool and the rest of the staff at Morgan and Claypool Publishers for their understanding, patience, and support in materializing this project.

This work was partly funded through the projects Integrated System for the Support of the Diagnosis for the Risk of Stroke (IASIS, 2002–2005), and Integrated System for the Evaluation of Ultrasound Imaging of the Carotid Artery (TALOS, 2003–2005), funded by the Research Promotion Foundation of Cyprus. Furthermore, partial funding and support was also obtained from the Cardiovascular Disease Educational and Research Trust (CDER Trust) of UK and Cyprus.

We hope that this book will be a useful reference for all the readers in this important field of research and contribute to the development and implementation of innovative imaging and video systems enabling the provision of better quality images.

Contents

CHAPTER 1

Introduction to Ultrasound Imaging and Speckle Noise

According to an old Chinese proverb, "a picture is worth a thousand words." In the modern age, this concept is still true for computer vision and image processing tasks, where we aim to derive better systems and tools that give us different perspectives on the same image, thus allowing us to understand not only its content but also its meaning and significance. Image processing cannot compete with the human eye in terms of accuracy, but it can perform better on observational consistency and ability to carry out detailed mathematical operations. In the course of time, image-processing research has evolved from basic low-level pixel operations to high-level analysis that now includes sophisticated techniques for image interpretation and analysis. These new techniques are being developed to gain a better understanding of images based on the relationships between its components, context, history, and knowledge gained from a range of sources.

The purpose of this chapter is to give a brief overview of ultrasound imaging and present its basic principles and limitations. Furthermore, speckle noise is introduced as a major noise factor, which limits image resolution and hinters further image processing analysis in ultrasound images. We then introduce different despeckle filtering techniques that may be applied as a preprocessing step for denoising of ultrasound images. A few examples of despeckle filtering for real ultrasound images are given, and some of its limitations are discussed. Finally, at the end of this chapter, we present the statistics of speckle noise and its mathematical model.

1.1 A BRIEF REVIEW OF ULTRASOUND IMAGING

Medical imaging technology has experienced a dramatic change in the last 30 years. Previously, only X-ray radiographs were available, which showed the organs as shadows on a photographic film. With the advent of modern computers and digital imaging technology, new imaging modalities like computer tomography (CT or computer-assisted tomography), magnetic resonance imaging (MRI), positron emission tomography (PET), and ultrasound, which deliver cross-sectional images of a patient's anatomy and physiology, have been developed. Among the imaging techniques

employed are X-ray angiography, X-ray, CT, ultrasound imaging, MRI, PET, and single photon emission computer tomography. MRI and CT have advantages over ultrasound imaging in the sense that higher resolution and clearer images are produced.

Imaging techniques have long been used for assessing and treating cardiac [67] and carotid disease [8, 24, 75]. Today's available imaging modalities produce a wide range of image data types for disease assessment, which include two-dimensional (2D) projection images, reconstructed three-dimensional (3D) images, 2D slice images, true 3D images, time sequences of 2D and 3D images, and sequences of 2D interior view (endoluminal) images. The use of ultrasound in the diagnosis and the assessment of imaging organs and soft tissue structures, as well as human blood, is well established [26] (see Figure 1.1, which illustrates two imaging scanners). Because of its noninvasive nature and continuing improvements in imaging quality, ultrasound imaging is progressively achieving an important role in the assessment and the characterization of cardiac imaging (see Figure 1.2), and the assessment of carotid artery disease [40, 53, 59, 60, 71, 75] (see Figure 1.3). The main disadvantage of ultrasound is that it does not work well in the presence of bone or gas, and the operator needs a high level of skill in both image acquisition and interpretation to carry out the clinical evaluation. On the other hand, standard angiography cannot give reliable information on the cross-sectional structure of the arteries [53]. This makes it difficult to accurately assess the build-up of plaque along the artery walls. B-mode ultrasound imaging or intravascular ultrasound (IVUS) has emerged, and it is widely used for visualizing carotid plaques and assessing plaque characteristics that are related to the onset of neurological symptoms. IVUS needs the insertion of a catheter into a vessel of interest that is equipped with an ultrasonic transducer enabling the reproduction of real-time cross-sectional images. However, reproducible measurements of the severity of the plaque in

(a) (b)

FIGURE 1.1: Ultrasound imaging scanners: (a) ATL™ HDI-5000 and (b) ATL™ Somnosite 180 plus portable ultrasound system [84].

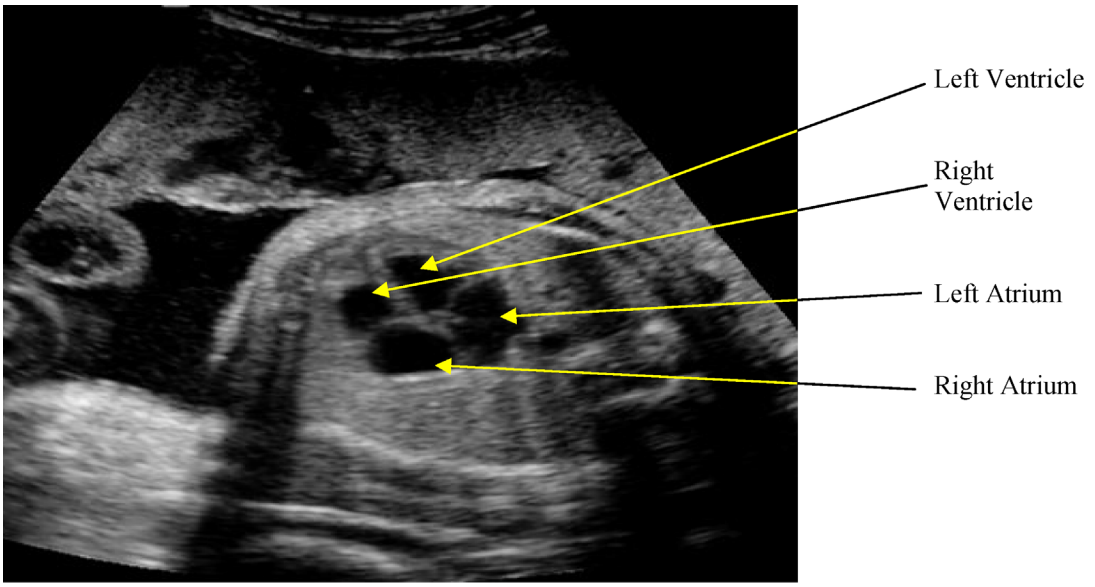

FIGURE 1.2: Ultrasound B-mode cardiac image, where the left ventricle (LV), the right ventricle (RV), the left atrium (LA), and the right atrium (RA) are indicated.

2D and 3D ultrasound are made difficult because of the complex shapes, the asymmetry of carotid plaques, and the speckle noise that is present in ultrasound images [26]. Furthermore, IVUS is an invasive method, as a catheter is inserted in the artery under investigation and possesses, therefore, a certain risk for the patient.

The use of ultrasound in medicine began during the Second World War in various centers around the world. The work of Dr. Karl Theodore Dussik in Austria in 1942 [85] on ultrasound transmission investigating the brain provides the first published work on medical ultrasonics. Furthermore, although other researchers in the United States, Japan, and Europe have also been cited as pioneers, the work of Prof. Ian Donald and his colleagues [86] in Glasgow, in the mid-1950s, did much to facilitate the development of practical ultrasound technology and applications. This led to the wider use of ultrasound in medical practice in subsequent decades.

From the mid-1960s onward, the advent of commercially available systems allowed the wider dissemination of the use of ultrasound. Rapid technological advances in electronics and piezoelectric materials provided further improvements from bistable to grayscale images and from still images to real-time moving images. The technical advances at this time (mid-1960s) led to the rapid growth in the applications of ultrasound. The development of Doppler ultrasound [87] has been progressing alongside the imaging technology, but the fusing of the two technologies in duplex scanning and the subsequent development of color Doppler imaging provided even more scope for investigating

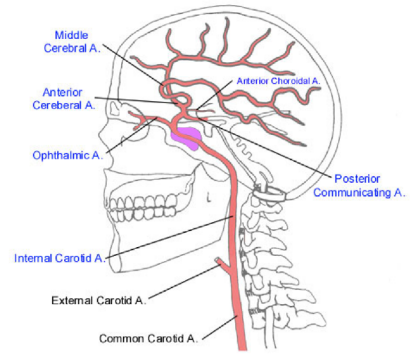
Middle
Cerebral A.
Anterior
Cereberal A.
Ophthalmic A.
Anterior Choroidal A.
Posterior
Communicating A.
Internal Carotid A.
External Carotid A.
Common Carotid A.

a)

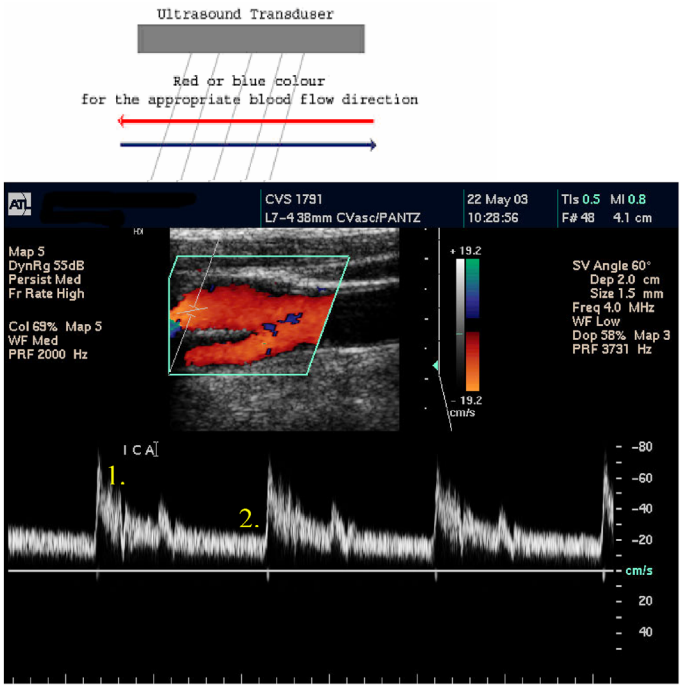
Ultrasound Transduser
Red or blue colour
for the appropriate blood flow direction
CVS 1791
L7-4 38mm CVasc/PANTZ
22 May 03
10:28:56
TIs 0.5 MI 0.8
F# 48 4.1 cm
Map 5
DynRg 55dB
Persist Med
Fr Rate High
Col 69% Map 5
WF Med
PRF 2000 Hz
+ 19.2
- 19.2
cm/s
SV Angle 60°
Dep 2.0 cm
Size 1.5 mm
Freq 4.0 MHz
WF Low
Dop 58% Map 3
PRF 3731 Hz
I C A
1.
2.
-80
-60
-40
-20
cm/s
20
40

b)

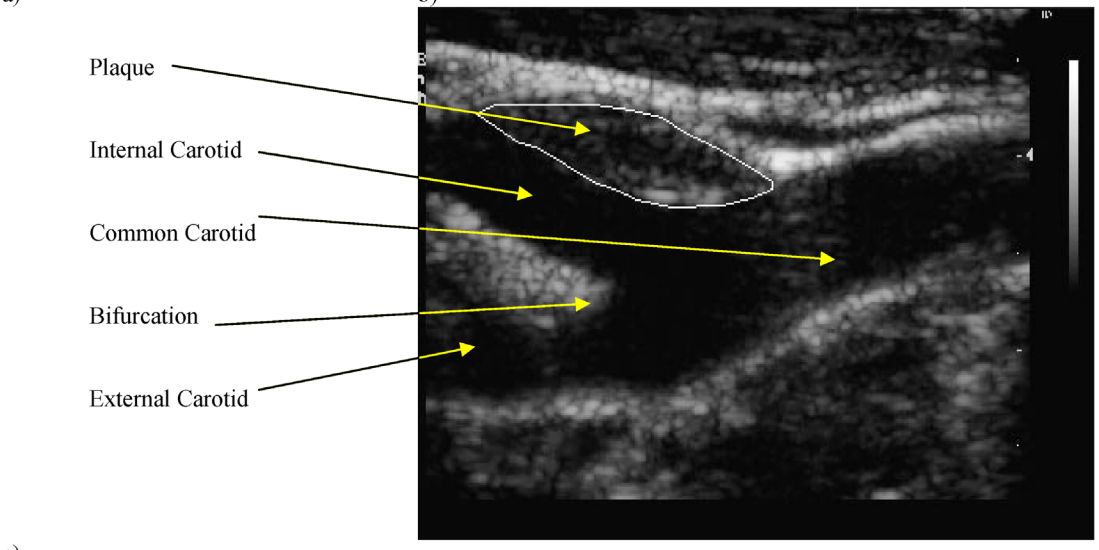
Plaque
Internal Carotid
Common Carotid
Bifurcation
External Carotid

c)

circulation and blood supply to organs, tumors, etc. The advent of the microchip in the 1970s and the subsequent exponential increase in processing power facilitated the development of faster and more powerful systems incorporating digital beam forming, signal enhancement, and new ways of interpreting and displaying data, such as power Doppler [87] and 3D imaging [46]. Ultrasound has long been recognized as a powerful tool for use in the diagnosis and the evaluation of many clinical entities. Over the past decade, as higher quality and less expensive scanners are widely available, ultrasound has proliferated throughout various specialties.

1.1.1 Basic Principles of Ultrasound Imaging

Ultrasound is a sound wave with a frequency that exceeds 20 kHz. It transports energy and propagates through several means as a pulsating pressure wave. It is described by a number of wave parameters such as pressure density, propagation direction, and particle displacement. If the particle displacement is parallel to the propagation direction, then the wave is called a longitudinal or compression wave. If the particle displacement is perpendicular to the propagation direction, it is a shear or transverse wave. The interaction of ultrasound waves with tissue is subject to the laws of geometrical optics. It includes reflection, refraction, scattering, diffraction, interference, and absorption. Except from interference, all other interactions reduce the intensity of the ultrasound beam.

The main characteristic of an ultrasound wave is its wavelength λ, which is a measure of the distance between two adjacent maximum or minimum values of a sine curve and its frequency f, which is the number of waves per unit of time. The product of these two measures gives the velocity of ultrasound wave propagation v described by the equation $v = f\lambda$. Ultrasound techniques are mainly based on measuring the echoes transmitted back from a medium when sending an ultrasound wave to it. In the echo impulse ultrasound technique, the ultrasound wave interacts with tissue and blood, and some of the transmitted energy returns to the transducer to be detected by

FIGURE 1.3: (a) The carotid system illustrating the common carotid artery, its bifurcation, and the internal and external carotid arteries [110]. (b) Longitudinal color flow duplex image of the carotid artery combined with the Doppler ultrasound image. The highlighted image with white contour on top shows the carotid bifurcation. The 2D signal shows the velocity variation that is related to the cardiac cycle. A blood flow velocity spectrum is displayed with markings 1 and 2, where marking 1 represents the peak systolic velocity, and marking 2 represents the end diastolic velocity. This is the duration of one cardiac cycle. Different colors (shades) represent blood flow direction. For the current picture, red represents the blood moving to the brain through the carotid artery, whereas blue represents the blood returning back from the brain. (c) Ultrasound B-mode longitudinal image of the carotid bifurcation with a manually outlined plaque, which is usually confirmed with the blood flow image. (For interpretation of the reference to color in this figure legend, the reader is referred to the Web version of this book.)

the instrument. If we know the velocity of propagation in the tissue under investigation, we can determine the distance from the transducer at which the interaction occurs [88]. The characteristics of the return signal (amplitudes, phases, etc.) provide information on the nature of the interaction, and, hence, they give some indication of the type of the medium in which they occurred. Mainly two principles are used in medical ultrasound diagnostics—the echo impulse technique and the Doppler technique [88].

The second principle used in ultrasound diagnostics is the Doppler principle, named after the physicist Christian Doppler (1803–1853) [89]. This technique is based on the principle that the received frequency of sound echoes reflected by a moving target is related to the velocity of the target. The frequency shift (the Doppler frequency shift) Δf of the echo signal is proportional to the flow velocity v (in centimeters per second) and the ultrasound transmission frequency f (in megahertz). The Doppler shift is described by the formula $\Delta f = 2f_0(v\cos\theta)/u_{sp}$, where f_0 is the transmitted frequency of the signal, θ is the angle between the direction of movement of the moving object and the ultrasound beam, and u_{sp} is the speed of sound through tissue that is approximately 1540 m/s.

In Doppler ultrasound, waves are produced by a vibrating crystal using the piezoelectric effect, whereas the returned echoes are displayed as a 2D signal, as shown in Figure 1.3b. When blood flow in a vessel is examined, sound reflections caused by the blood's corpuscular elements play a major role. Based on the fact that blood flow velocity varies in different areas of a vessel, the Doppler signal contains a broad frequency spectrum. In a normal internal carotid artery (ICA), the spectrum varies from 0.5 to 3.5 kHz, and v is less than 120 cm/s when an ultrasound beam of 4 MHz is used.

1.1.2 Ultrasound Modes

The two main scanning modes are A- and B-modes. Other modes used are M-mode, duplex ultrasound, color-coded ultrasound, and power Doppler ultrasound, which will be briefly introduced below.

A-mode refers to amplitude mode scanning, which is mainly of historical interest. In this mode, the strength of the detected echo signal is measured and displayed as a continuous signal in one direction. A-mode is a line, with strong reflections being represented as an increase in the signal amplitude. This scanning technique has the limitation that the recorded signal is 1D with limited anatomical information. A-mode is no longer used, especially for the assessment of cardiovascular disease. Its use is restricted to very special uses such as in ophthalmology to perform very accurate measurements of distance.

B-mode refers to the brightness mode. In B-mode, echoes are displayed as a 2D grayscale image. The amplitude of the returning echoes is represented as dots (pixels) of an image with different gray values, as illustrated in Figure 1.3b and 1.3c. The image is constructed by these pixels line

by line. Advances in B-mode ultrasound have resulted in improved anatomic definition, which has enabled plaque characterization [39, 88].

M-mode is used in cardiology, and it is actually an A-scan plotted against time. The result is the display of consecutive lines plotted against time. Using this mode, detailed information may be obtained about various cardiac dimensions and also the accurate timing of vascular motion.

Moving blood (see Figure 1.3b) generates a Doppler frequency shift in the reflected sound from insonated red blood cells, and this frequency shift can be used to calculate the velocity of the moving blood using the Doppler equation [89]. The invention of gated Doppler ultrasound in the late 1950s allowed velocity sampling at different depths and positions, and its subsequent combination with B-mode real-time ultrasonic imaging led to the development of duplex ultrasound. Stenosis in any vessel is characterized by an increase in systolic and diastolic velocities. Several types of Doppler systems are used in medical diagnosis: continuous wave (CW) Doppler, pulsed wave (PW) Doppler, duplex ultrasound, and color flow duplex (see also Figure 1.3b). In CW Doppler, the machine uses two piezoelectric elements serving as transmitters and receivers. They continuously transmit ultrasound beams. Because of the continuous way that ultrasound is being transmitted, no specific information about depth can be obtained. PW Doppler is used to detect blood flow at a specific depth. Sequences of pulses are transmitted to the human body, which are gated for a short period of time to receive the echoes. By selecting the time interval between the transmitted and received pulses, it is possible to examine vessels at a specific depth.

In color-coded ultrasound, every pixel is tested for Doppler shift. Using this technique, the movement of the red blood cells is finally depicted through color. The final image results by superimposing the color-coded image on the B-mode image.

Power Doppler is the depiction of flow based on the integrated power of the Doppler spectrum rather than on the mean Doppler frequency. This modality results in an angle, which is independent of the resulting enhanced sensitivity in flow detection as compared to the color-coded Doppler, and, therefore, the detection of low flow is better viewed.

1.1.3 Image Quality and Resolution

The quality of the produced ultrasound image depends on image resolution, axial and lateral. Resolution is defined as the smallest distance between two points at which they can be represented as distinct. Axial resolution refers to the ability of representing two points that lie along the direction of ultrasound propagation. It depends on the wavelength of the beam. In B-mode, ultrasound pulses consist of one to two sinusoidal wavelengths, and the axial resolution is dependent on the wavelength of the waveforms and lies in the range of the ultrasound wavelength λ ($\lambda = 0.21$ mm). Resolution depends on the frequency of the beam waveforms. Since this value is reciprocal to the ultrasound frequency ($\lambda = v / f$), the axial resolution improves with increasing frequency.

Lateral resolution refers to the ability to represent two points that lie at a right angle to the direction of ultrasound propagation. This is dependent on the width of the ultrasound wave (beam). To be able to resolve points that lie close together, the width of the ultrasound beam has to be kept reasonably small, and the diameter of the transducer is kept as large as possible (i.e., small phase-array transducers have worse lateral resolution than large linear or curved-array transducers).

To achieve the best results in vascular ultrasound imaging, the transmission frequencies are in the range of 1–10 MHz. The selected frequency depends on the application domain. For arteries that are located close to the human skin, frequencies greater than 7.5 MHz are used, whereas for arteries that are located deeper in the human body, frequencies from 3 to 5 MHz are used. For transcranial applications, frequencies less than 2 MHz are used. However, when selecting a frequency, the user has to keep in mind that the axial resolution is proportional to the ultrasound wavelength, whereas the intensity of the signal depends on the attenuation of the signal transmitted through the body, with the higher the frequency, the higher the attenuation. Therefore, there is a tradeoff between higher resolution ultrasound images at smaller depths and lower resolution images at higher depths.

1.1.4 Limitations of Ultrasound Imaging

Variability in B-mode images (even when using the same ultrasonic equipment with fixed settings) does exist [75]. Sources of variability are outlined below.

1. Geometrical and diffraction effects, where spatial compound imaging may be employed to correct the image [39, 89].
2. Interpatient variation due to depth dependence and inhomogeneous intervening tissue, where normalization techniques may be applied to standardize the image [54, 55, 59, 60].
3. Speckle noise affecting the quality of ultrasound B-mode imaging. It is described as an ultrasound textural pattern that varies depending on the type of the biological tissue. The presence of speckle, which is difficult to suppress [5–28], may obscure small structures, thus degrading the spatial resolution of an ultrasonic image [59]. Despeckle filtering may be applied to improve the quality of the image.
4. Low contrast of the intima media complex or plaque borders [24, 53] and a small thin size [54, 60], making the image interpretation a difficult task.
5. Falsely low echogenicity due to shadowing effects, hindering the observation in B-mode images, of plaques or the intima media complex or other structures [53].
6. Low signal-to-noise ratio (SNR) in anechoic components and difficulty in outlining the carotid plaque, or other tissue under investigation, where the difficulty may be overcome by employing the use of color-coded images [54, 55].
7. Intraobserver variability where the ultrasound images inspected by the same expert at different occasions might be differently evaluated [59, 60].

8. Interobserver variability where the ultrasound images inspected by two or more experts might be differently evaluated [59].

It is noted that entries 7 and 8 are applicable in any medical imaging modality. To overcome intraobserver and interobserver variability, it is generally recommended that multiple observers should perform the image evaluation.

1.2 SPECKLE NOISE

In this section, we introduce speckle noise as a major factor limiting visual perception and processing of ultrasound [and synthetic aperture radar (SAR) images] [2–4, 9]. A mathematical speckle model for ultrasound images is introduced, where the statistics of speckle noise are presented, taking into consideration the log compression of the ultrasound image, which is performed to match the image into the display device (see Section 1.2.2). Based on this speckle model, a number of despeckling techniques are derived and explained in detail in Chapter 2. Specifically, the following categories of despeckle filtering techniques are presented: linear filtering (local statistics filtering, homogeneity filtering), nonlinear filtering (median filtering, linear scaling filtering, geometric filtering, logarithmic filtering, homomorphic filtering), anisotropic diffusion filtering (anisotropic diffusion, speckle-reducing anisotropic diffusion, coherent nonlinear anisotropic diffusion), and wavelet filtering.

Noise and artifacts can cause signal and image degradation for many medical image modalities. Different image modalities exhibit distinct types of degradation. Images formed with coherent energy, such as ultrasound, suffer from speckle noise. Image degradation can have a significant impact on image quality and, thus, affect human interpretation and the accuracy of computer-assisted methods. Poor image quality often makes feature extraction, analysis, recognition, and quantitative measurements problematic and unreliable. Therefore, image despeckling is a very important task, which motivated a significant number of studies in medical imaging [14, 22–24, 26, 28, 31].

The use of ultrasound in the diagnosis and the assessment of arterial disease is well established because of its noninvasive nature, its low cost, and the continuing improvements in image quality [1]. Speckle is a form of locally correlated multiplicative noise that corrupts medical ultrasound imaging making visual observation difficult [2, 3]. The presence of speckle noise in ultrasound images has been documented since the early 1970s, where researchers such as Burckhardt [2], Wagner et al. [3], and Goodman [4] described the fundamentals and the statistical properties of the speckle noise. Speckle is not truly noise in the typical engineering sense since its texture often carries useful information about the image being viewed [2–4].

Speckle noise is the primary factor that limits the contrast resolution in diagnostic ultrasound imaging, thereby limiting the detectability of small low-contrast lesions and making the ultrasound images generally difficult for the nonspecialist to interpret [2, 3, 5, 6]. Because of the

speckle presence, ultrasound experts with sufficient experience may not often draw useful conclusions from the images [6]. Speckle also limits the effective application (e.g., edge detection) of automated computer-aided analysis (e.g., volume rendering, 3D display) algorithms. It is caused by the interference between ultrasound waves reflected from microscopic scattering through the tissue.

Therefore, speckle is most often considered a dominant source of noise in ultrasound imaging and should be filtered out [2, 5, 6] without affecting important features of the image. In this book, we carry out a comparative evaluation of despeckle filtering techniques based on texture analysis, image quality evaluation metrics, as well as visual assessment by experts on 440 ultrasound images of the carotid artery bifurcation. Results of this study were also published in Ref. [7]. Moreover, a comparative evaluation framework for the selection of the most appropriate despeckle filter for the problem under investigation is proposed.

1.2.1 Physical Properties and the Pattern of Speckle Noise

The speckle pattern, which is visible as the typical light and dark spots the image is composed of, results from destructive interference of ultrasound waves scattered from different sites. The nature of speckle has been a major subject of investigation [2–4, 12, 31]. When a fixed rigid object is scanned twice under exactly the same conditions, one obtains identical speckle patterns. Although of random appearance, speckle is not random in the same sense as electrical noise. However, if the same object is scanned under slightly different conditions, say, with a different transducer aperture, pulse length, or transducer angulation, the speckle patterns change.

The most popular model adopted in the literature to explain the effects that occur when a tissue is insonated is illustrated in Figure 1.4, where a tissue may be modeled as a sound absorbing medium containing scatterers, which scatter the sound waves [56, 83]. These scatterers arise from inhomogeneity and structures approximately equal to or smaller in size than the wavelength of the ultrasound, such as tissue parenchyma, where there are changes in acoustic impedance over a microscopic level within the tissue. Tissue particles that are relatively small in relation to the wavelength (i.e., blood cells), and particles with differing impedance that lie very close to one another, cause scattering or speckling. Absorption of the ultrasound tissue is an additional factor to scattering and refraction, responsible for pulse energy loss. The process of energy loss involving absorption, reflection, and scattering is referred to as attenuation, which increases with depth and frequency. Because a higher frequency of ultrasound results in increased absorption, the consequence is a decrease in the depth of visualization.

Figure 1.5 illustrates the entire scattering procedure [56]. Consider a transducer insonating a homogeneous medium containing four point-like scatterers, as depicted in Figure 1.5a. These scatterers yield spherical waves that will arrive at the transducer at slightly different times after the transmission of the ultrasound pulse. Usually, the pulse envelope is approximately Gaussian,

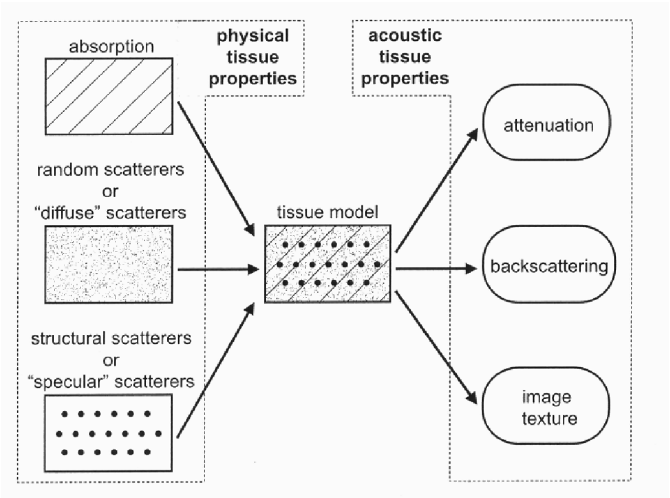

FIGURE 1.4: The usual tissue model in ultrasound imaging (modified from Ref. [56]).

as shown in Figure 1.5b. If the pulse has a Gaussian shape, then so is its spectrum. One chooses a Gaussian shape because for a medium with a linear attenuation coefficient, this Gaussian shape of the spectrum is maintained while the pulse travels through the medium (although a shift of this Gaussian spectrum to lower frequencies occurs while the pulse travels through the medium because the attenuation increases with the frequency).

Upon reception of the reflected signal, the transducer produces an electrical signal [radio frequency (RF)] that is the algebraic sum of the instantaneous sound pressures originating from the backscattered waves (four waves in Figure 1.5a). The depth differences of the scatterers are smaller than the axial size of the resolution volume of the transducer (i.e., the pulse length). This is, in fact,

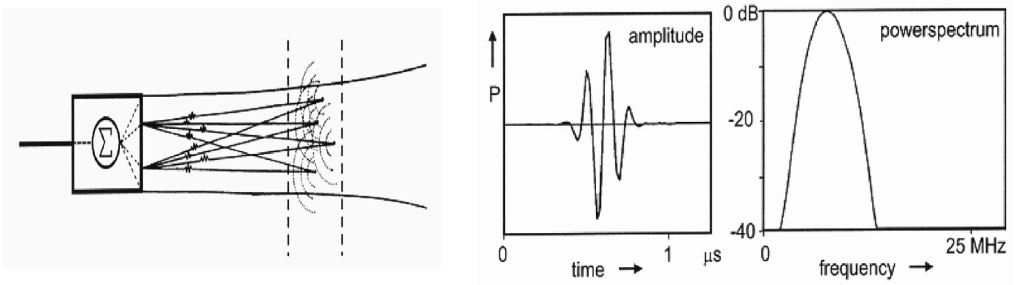

(a) (b)

FIGURE 1.5: (a) The scattering in the sound beam. (b) One pulse in the time and frequency domains (from Ref. [56]).

the basic cause for the generation of tissue texture. The formed pattern is the so-called speckle pattern. Note, in particular, that the tissue texture resulting from this speckle pattern is, in general, not a true image of the histological structure of the tissue, but rather an interference pattern that is mainly determined by the beam characteristics. Speckle is described as one of the more complex image noise models [3, 4, 31, 56]; it is signal dependent, non-Gaussian, and spatially dependent.

In homogeneous tissue, the distribution of the scatterers throughout the 3D space is assumed to be isotropic. As displayed in Figure 1.4, one distinguishes random (or diffuse) scatterers and structural (or specular) scatterers. The diffuse scatterers are assumed to be uniformly distributed over space. Diffuse scattering arises when there are a number of scatterers with a random phase within the resolution cell of the ultrasound beam. This random nature of the location of the scatterers causes the statistical nature of the echo signals and, hence, the resulting speckle pattern. Consequently, a statistical approach to its analysis seems obvious.

Other properties of the tissue that affect the ultrasound as it propagates through it are the propagation speed, the attenuation, and the backscattering. The absorption of ultrasound is caused by relaxation phenomena of biological macromolecules [58] that transfer mechanical energy into heat. Another source of attenuation is the scattering, i.e., omnidirectional reflections by small inhomogeneity in the tissue. The overall attenuation is, therefore, the result of absorption and scattering (as illustrated in Figure 1.4), which are both frequency dependent in such a way that the attenuation increases with frequency.

In analyzing speckle, an important point to bear in mind is to make a clear distinction between the speckle as it appears in the image and the speckle in the received RF signal. The block diagram in Figure 1.6 explains the entire track of the RF signal from the transducer to the screen inside the ultrasound imaging system. As set forth, the signal is subject to several transformations that severely affect its statistics. The most important of these is the log compression of the signal, which is employed to reduce the dynamic range of the input signal to match the lower dynamic range of the display device. The input signal could have a dynamic range of the order of 50–70 dB, whereas a typical display could have a dynamic range of the order of 20–30 dB. Such a relation is normally affected through an amplifier, which has a reducing amplification for a larger input signal.

In addition, the expert has the possibility to manually adjust several machine settings. In Figure 1.6, these are indicated as the slide contact overall gain and the time gain compensation (TGC). These machine settings control the amplification of the signal—the overall gain controls the overall amplification, and the TGC is a time-dependent amplification—and serve as tools for the expert to adjust the image for an optimal visual diagnosis. The TGC is adjusted by several (usually seven) slide contacts, each of which controls the gain in part of the image. For instance, if the slide contacts are placed in a vertical row, the top slide contact controls the gain in the top of the image, the bottom slide contact controls the gain in the bottom of the image, etc. This position-specific gain in

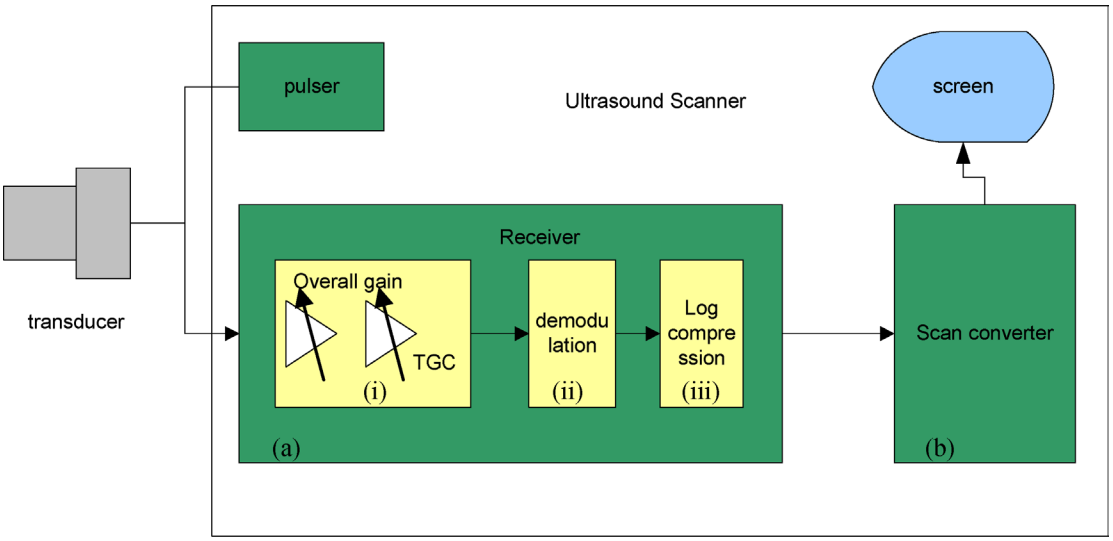

FIGURE 1.6: The processing steps of the RF signal inside the ultrasound scanner (modified from Ref. [57]).

the image is realized by making the amplification of the signal dependent on the exact time that the sound reflection is received. Since the position where a pixel is displayed on the screen is dependent on this time instant, the time-dependent amplification of the received signal converts to a position-dependent change in the gray value of the pixels on the screen.

1.2.2 Speckle Noise Modeling

To be able to derive an efficient despeckle filter, a speckle noise model is needed. The speckle noise model for both ultrasound and SAR images may be approximated as multiplicative [31]. The signal at the output of the receiver demodulation module of the ultrasound imaging system [see Figure 1.6a(ii)] may be defined as

$$y_{i,j} = x_{i,j} n_{i,j} + a_{i,j}, \tag{1.1}$$

where $y_{i,j}$ represents the noisy pixel in the middle of the moving window, $x_{i,j}$ represents the noise-free pixel, $n_{i,j}$ and $a_{i,j}$ represent the multiplicative and additive noise, respectively, and i,j are the indices of the spatial locations that belong in the 2D space of real numbers, $i,j \in \Re^2$.

Despeckling is based on estimating the true intensity $x_{i,j}$ as a function of the intensity of the pixel $y_{i,j}$ and some local statistics calculated on a neighborhood of this pixel.

Wagner et al. [3] showed that the histogram of amplitudes within the resolution cells of the envelope-detected RF signal backscattered from a uniform area with a sufficiently high scatterer

density has a Rayleigh distribution with mean μ proportional to the standard deviation σ (with $\mu/\sigma = 1.91$). This implies that speckle could be modeled as multiplicative noise.

However, the signal processing stages inside the scanner modify the statistics of the original signal, i.e., the logarithmic compression [see Figure 1.6a(iii)]. The logarithmic compression is used to adjust the large echo dynamic range (50–70 dB) to the number of bits (usually 8) of the digitization module in the scan converter (see Figure 1.6b). More specifically, logarithmic compression affects the high-intensity tail of the Rayleigh and Rician probability density functions more than the low-intensity part. As a result, the speckle noise becomes very close to the white Gaussian noise corresponding to the uncompressed Rayleigh signal [31]. In particular, it should be noted that speckle is no longer multiplicative in the sense that, on homogeneous regions, where $x_{i,j}$ can be assumed constant, the mean is proportional to the variance ($\mu \approx \sigma^2$) rather than the standard deviation ($\mu \approx \sigma$) [24, 26, 28, 31]. In this respect, the speckle index C will be for the log-compressed ultrasound images, i.e., $C = \sigma^2/\mu$.

Referring back to Eq. (1.1), since the effect of the additive noise is considerably smaller compared with that of the multiplicative noise, it may be written as

$$y_{i,j} \approx x_{i,j} n_{i,j}. \tag{1.2}$$

Thus, the logarithmic compression transforms the model in Eq. (1.2) into the classical signal in the additive noise form as

$$\log(y_{i,j}) = \log(x_{i,j}) + \log(n_{i,j}) \tag{1.3}$$

and

$$g_{i,j} = f_{i,j} + nl_{i,j}. \tag{1.4}$$

For the rest of the book, the term $\log(y_{i,j})$, which is the observed pixel on the ultrasound image display after logarithmic compression, is denoted as $g_{i,j}$, and the terms $\log(x_{i,j})$ and $\log(n_{i,j})$, which are the noise-free pixel and the noise component after logarithmic compression, are denoted as $f_{i,j}$ and $nl_{i,j}$, respectively [see Eq. (1.4)].

1.2.3 Early Attempts of Despeckle Filtering in Different Modalities and Ultrasound Imaging

The widespread of ultrasound imaging equipment, including mobile and portable telemedicine ultrasound scanning instruments and computer-aided systems, necessitates the need for better image processing techniques to offer a clearer image to the medical practitioner. This makes the use of efficient despeckle filtering a very important task. Early attempts to suppress speckle noise were

implemented by averaging of uncorrelated images of the same tissue recorded under different spatial positions [5, 9, 10]. Although these methods are effective for speckle reduction, they require multiple images of the same object to be obtained [11]. Speckle-reducing filters originated from the SAR community [9]. These filters then have later been applied to ultrasound imaging since the early 1980s [12]. Filters that are widely used in both SAR and ultrasound imaging were originally proposed by Lee [9, 14, 15], Kuan et al. [11], Frost et al. [13], and Kuan and Sawchuk [16].

Some researchers have tried in the past to despeckle SAR images by averaging of uncorrelated images obtained from different spatial positions [46]. These temporal averaging and multiframe methods aimed to increase the SNR by generating multiple uncorrelated images that are incoherently summed to reduce speckle [82]. Despite being simple and fast, these approaches suffer from two limitations. First, to produce uncorrelated ultrasound images, the transducer has to be translated at least by about half its element width for each of the generated frames [2]. Second, temporal averaging based on transducer movement causes the loss of small details such as small vessels and texture patterns because of blurring. For the above reasons, this procedure has been proven to be not suitable for despeckle filtering. It is most suitable for additive noise reduction [46, 82]. Another disadvantage of this method is that multiple images from the same object are required [10, 15]. Other researchers applied their techniques on the ultrasound images of the kidney [26], echocardiograms [27], heart [24], abdomen [24], pig heart [28], and liver [63], on SAR images [17, 34, 77, 78], and on real-world [16, 28] and artificial images [10, 66]. They used statistical measures, like the mean, the variance, the median, the speckle index (C), the mean-square error (MSE), the image contrast, and the visual perception evaluation made by experts, to evaluate their techniques. They compared their despeckling techniques with the Lee filter [9], homomorphic filtering [17, 18], the median filter [33], and diffusion filtering [5, 20–23]. Despeckle filtering can also be used as a preprocessing step for image segmentation [7, 54, 59, 60] or image registration [46] techniques. By suppressing the speckle, the performance of these techniques can be improved.

Many authors have shown a reduction of lesion detectability of approximately a factor of 8 due to the presence of speckle noise in the image [2, 4, 13]. This radical reduction in contrast resolution is responsible for the poorer effective resolution of ultrasound compared to X-ray and MRI [46]. Despeckle filtering is, therefore, a critical preprocessing step in medical ultrasound images provided that the features of interest for the diagnosis are not lost.

1.3 AN OVERVIEW OF DESPECKLE FILTERING TECHNIQUES

Table 1.1 summarizes the despeckle filtering techniques for ultrasound imaging that are presented in this book, grouped under the following categories: linear filtering (local statistics filtering, homogeneity filtering), nonlinear filtering (median filtering, linear scaling filtering, geometric filtering,

TABLE 1.1: An overview of despeckle filtering techniques

SPECKLE REDUCTION TECHNIQUE	METHOD	INVESTIGATOR	FILTER NAME
Linear filtering	Moving window utilizing local statistics		
	1. Mean (μ) and variance (σ^2)	[9–14] and [13–16]	*DsFlsmv*
	2. Mean, variance, third and fourth moments (higher statistical moments) and entropy	[9–14]	*DsFlsmvsk1d* *DsFlsmvsk2d*
	3. Homogeneous mask area filters	[32]	*DsFlsminsc*
	4. Wiener filtering	[2–15]	*DsFwiener*
Nonlinear filtering	Median filtering	[33]	*DsFmedian*
	Linear scaling of the gray-level values	[46]	*DsFls* *DsFca* *DsFlecasort*
	Based on the most homogeneous neighborhood around each pixel	[8]	*DsFhomog*
	Nonlinear iterative algorithm (geometric filtering)	[10]	*DsFgf4d*
	The image is logarithmically transformed, the FFT is computed and denoised, and the inverse FFT is computed and finally exponentially transformed back	[2, 17, 18]	*DsFhomo*
Diffusion filtering	Nonlinear filtering technique for simultaneously performing contrast enhancement and noise reduction	[2, 5, 12, 13, 19–23]	*DsFad*
	Exponential damp kernel filters utilizing diffusion	[5]	

TABLE 1.1: (*continued*)

SPECKLE REDUCTION TECHNIQUE	METHOD	INVESTIGATOR	FILTER NAME
	Speckle-reducing anisotropic diffusion based on the coefficient of variation	[24]	*DsFsrad*
	Coherence enhancing diffusion	[24]	*DsFnldif*
Wavelet filtering	Only the useful wavelet coefficients are utilized	[15, 25–29, 35]	*DsFwaveltc*

logarithmic filtering, homomorphic filtering), anisotropic diffusion filtering (anisotropic diffusion, speckle-reducing anisotropic diffusion, coherent nonlinear anisotropic diffusion), and wavelet filtering. Furthermore, in Table 1.1, the methodology used, the main investigators, and the corresponding filter names are given. These filters are briefly introduced in this chapter and presented in detail in Chapter 2.

Some of the linear filters are Lee [9, 14, 15], Frost [13], and Kuan [11, 16]. The Lee and Frost filters have the same structure, whereas the Kuan filter is a generalization of the Lee filter. Both filters form the output image by computing the central pixel intensity inside a filter-moving window, which is calculated from the average intensity values of the pixels and a coefficient of variation inside the moving window. Kuan considered a multiplicative speckle model and designed a linear filter based on the minimum-mean-square error criterion that has optimal performance when the histogram of the image intensity is Gaussian distributed. The Lee filter [9] is a particular case of the Kuan filter based on a linear approximation made for the multiplicative noise model. The Frost filter [13] makes a balance between the averaging and the all-pass filters. It was designed as an adaptive Wiener filter that assumed an autoregressive exponential model for the image.

In the nonlinear filtering group, the gray-level values are linearly scaled to despeckle the image [61]. Some of the nonlinear filters are based on the most homogeneous neighborhood around each image pixel [8]. Geometric filters [10] are based on nonlinear iterative algorithms, which increment or decrement the pixel values in a neighborhood based on their relative values. The method of homomorphic filtering [17, 18] is similar to the logarithmic point operations used in histogram enhancement, where dominant bright pixels are de-emphasized. In the homomorphic filtering, the fast Fourier transform (FFT) of the image is calculated and then denoised, and then the inverse FFT is calculated.

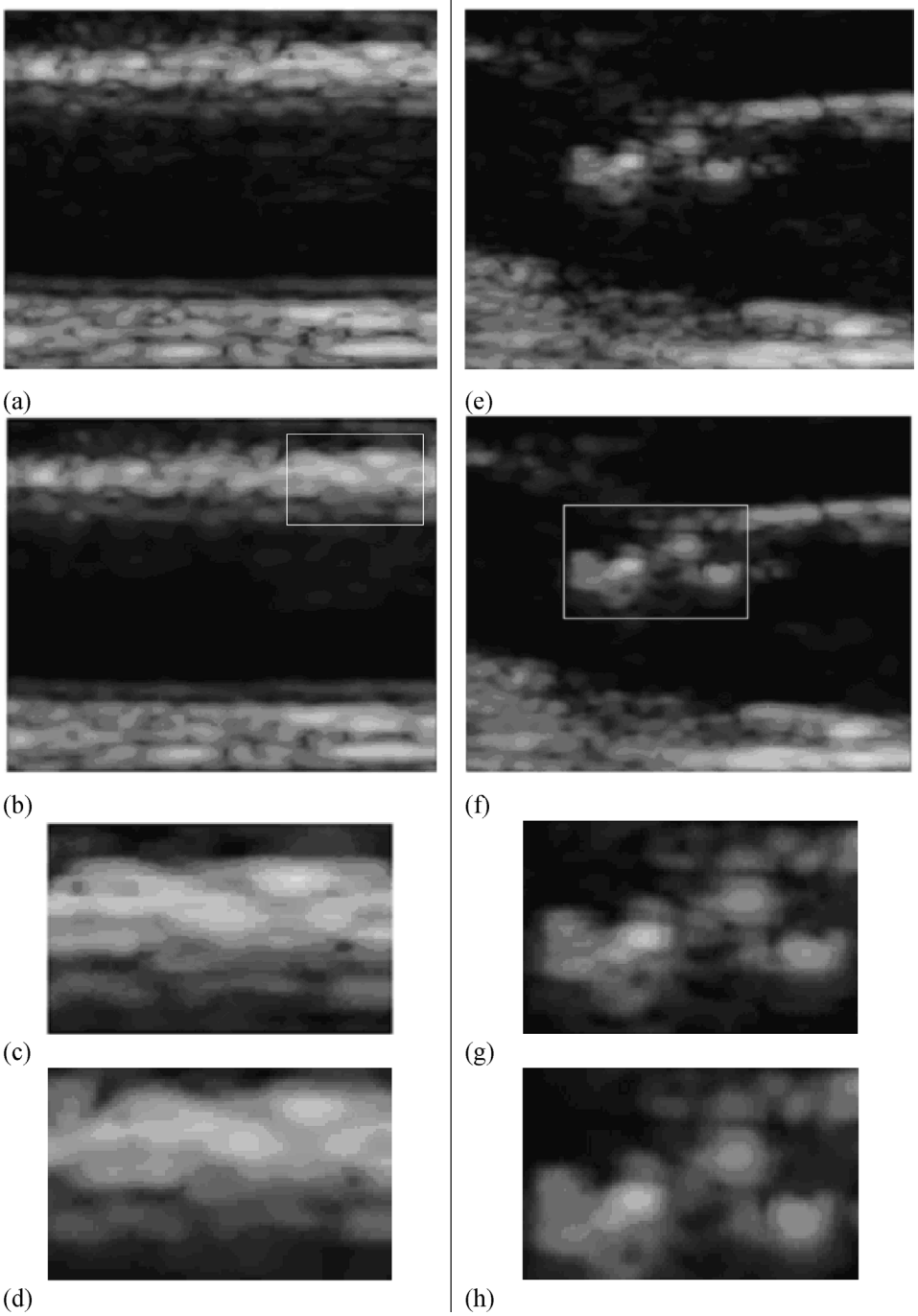
(a)
(e)
(b)
(f)
(c)
(g)
(d)
(h)

The diffusion filtering category includes filters based on anisotropic diffusion [2, 19, 20–23], coherence anisotropic diffusion [24], and speckle-reducing anisotropic diffusion [5]. These filters have been recently presented in the literature and are nonlinear filtering techniques. They simultaneously perform contrast enhancement and noise reduction by utilizing the coefficient of variation [5]. Furthermore, in the wavelet category, filters for suppressing the speckle noise were documented. These filters are making use of a realistic distribution of the wavelet coefficients [2, 15, 25–30], where only the useful wavelet coefficients are utilized. Different wavelet shrinkage approaches were extensively investigated based on Donoho's work [29].

Figure 1.7 illustrates original longitudinal asymptomatic (see Figure 1.7a) and symptomatic images (see Figure 1.7e) and their despeckled images (see Figure 1.7b and 1.7f). Asymptomatic images were recorded from patients at risk of atherosclerosis in the absence of clinical symptoms, whereas symptomatic images were recorded from patients at risk of atherosclerosis, which have already developed clinical symptoms, such as a stroke episode. Figure 1.7c–1.7h shows an enlarged window from the original and despeckled images (shown in a rectangle in Figure 1.7b and 1.7f).

1.4 LIMITATIONS OF DESPECKLE FILTERING TECHNIQUES

Despeckling is always a tradeoff between noise suppression and loss of information, which is something that experts are very concerned about. It is, therefore, desirable to keep as much important information as possible. The majority of speckle reduction techniques have certain limitations that can be briefly summarized as follows.

1. They are sensitive to the size and the shape of the window. The use of different window sizes greatly affects the quality of the processed images. If the window is too large, oversmoothing will occur, subtle details of the image will be lost in the filtering process, and edges will be blurred. On the other hand, a small window will decrease the smoothing capability of the filter and will not reduce the speckle noise, thus making the filter not effective. In homogenous areas, the larger the window size, the more efficient the filter in reducing the speckle noise. In heterogeneous areas, the smaller the window size, the more it is possible to keep subtle image details unchanged. Our experiments showed that a $[7 \times 7]$ window size is a fairly good choice.
2. Some of the despeckle methods based on window approaches require thresholds to be

FIGURE 1.7: Results of despeckle filtering based on linear filtering (first-order local statistics, *DsFlsmv*). Asymptomatic case: (a) original, (b) despeckled, (c) enlarged region marked in (b) of the original, and (d) enlarged region marked in (b) of the despeckled image. Symptomatic case: (e) original, (f) despeckled, (g) enlarged region marked in (f) of the original, (h) enlarged region marked in (f) of the despeckled image. Regions were enlarged by a factor of 3.

used in the filtering process, which have to be empirically estimated. There are a number of thresholds introduced in the literature, which include gradient thresholding [5], soft or hard thresholds [29], nonlinear thresholds [28], and wavelet thresholds [25, 28, 37]. The inappropriate choice of a threshold may lead to average filtering and noisy boundaries, thus leaving the sharp features unfiltered [7, 10, 14].

3. Most of the existing despeckle filters do not enhance the edges, but they only inhibit smoothing near the edges. When an edge is contained in the filtering window, the coefficient of variation will be high, and smoothing will be inhibited. Therefore, speckle in the neighborhood of an edge will remain after filtering. They are not directional in the sense that in the presence of an edge, all smoothing is precluded. Instead of inhibiting smoothing in directions perpendicular to the edge, smoothing in directions parallel to the edge is allowed.
4. Different evaluation criteria for evaluating the performance of despeckle filtering are used by different studies. Although most of the studies use quantitative criteria like the MSE and the speckle index (C), there are additional quantitative criteria like texture analysis and classification, image quality evaluation metrics, and visual assessment by experts that could be investigated.

1.5 GUIDE TO BOOK CONTENTS

In the following chapter, the theoretical background (equations), the algorithmic steps, and the MATLAB™ code of despeckle filters given in Table 1.1 are presented. Chapter 3 covers the evaluation methodology, the material and recording of ultrasound images, the texture and statistical analysis, the statistical k-nearest-neighbor classifier, the image quality evaluation metrics, and the experiments carried out for visual evaluation. Chapter 4 presents the applications of despeckle filtering techniques in ultrasound images of the carotid artery and in cardiac ultrasound images. Chapter 5 discusses, compares, and evaluates the proposed despeckle filtering techniques, where the strong and weak points for each filtering technique are presented. Reference is also made to video despeckling, where a video despeckling protocol is presented. Chapter 6 presents the summary and future directions, where a despeckling filtering and evaluation protocol is also proposed.

Finally, at the end of this book, an appendix provides additional information of all the functions used in this book, as these will be introduced in Chapter 2 and Chapter 3, together with the MATLAB™ code. Section A.2 of the appendix illustrates examples in MATLAB code for running the despeckle filtering toolbox functions.

• • • •

List of Symbols

$a_{i,j}$	Additive noise component on pixel i,j
α_{comp}, β_{comp}	Logarithmic compression parameters
$\beta(s)$	Snake stiffness of the energy functional
β_{GVF}	GVF snake rigidity parameter
C	Speckle index
CV%	Coefficient of variation
$cd(\|\nabla g\|)$, $c_{i,j}$	Diffusion coefficient
c_{adsr}	Speckle reducing anisotropic diffusion coefficient
c	Constant controlling the magnitude of the potential
$c_{s\,sin\_1}$, $c_{s\,sin\_2}$	Constants used to calculate the SSIN
c_2	Positive weighting factor
Γ	Number of directions, which diffusion is computed
γ	Signal-to-noise radio (SNR)
$D \in \Re^{2x2}$	Symmetric positive semi-definite diffusion tensor representing the required diffusion in both gradient and contour directions
D_f	Fractal dimension
D	Matrix used to calculated the image energy of the snake, $E_{image}(v)$
$D_{viewing}$	Viewing distance
DR	Dynamic range of input ultrasound signal
$d(k)$	Wavelet coefficient for the wavelet filtering
Δf	Frequency shift (Doppler frequency shift)
Δr	Distance between two pixels
∇g	The gradient magnitude of image $g(x,y)$(gradient)
$\nabla g_{i,j}$	Directional derivative (simple difference) at location i,j
$f_1 \cdots f_{13}$	SGLDM texture measures from Haralick
$f_x(x,y)$	First-order differential of the edge magnitude along the x-axis
$f_{i,j}$	Noise-free signal ultrasound signal in discrete form (the new image) on pixel i,j
f	Frequency of ultrasound wave
f_0	Transmitted frequency of ultrasound signal

$feat\_dis_i$	Percentage distance
$g_{i,j}$	Observed ultrasound signal in discrete formulation after logarithmic compression
$g(x,y)$	Observed ultrasound signal after logarithmic compression, representing image intensity at location (x, y)
G	Linear gain of the amplifier
$G\sigma * g_{i,j}$	Image convolved with Gaussian smoothing filter
$G\sigma$	Gaussian smoothing filter
$\overline{g}_i, \overline{f}_i$	Mean gravity of the searching pixel region in image g or f
$g_{\max}$ and $g_{\min}$	Maximum and minimum gray-level values in a pixel neighborhood, respectively
Ha, kHz, and MHz	Hertz, kilohertz, and megahertz, respectively
HX, HY	Entropies of p_x and p_y
$H^{(k)}$	Hurst coefficients
$H(x,y)$	Array of points of the same size for the HT
HD	Hausdorff distance
η_s	Spatial neighborhood of pixel i, j
$\lvert\eta_s\rvert$	Number of neighbors (usually four except at the image boundaries)
θ_i	Phase shift relative to the insonated ultrasound wave
θ	Angle between the direction of movement of the moving object and the ultrasound beam
I	Identity matrix
$I_0(x)$	Modified Bessel function of the first kind of order 0
$I_1 - I_7$	Echo boundaries describing the regions in carotid artery
IMT_{mean}	Mean value of the IMT
IMT_{min}	IMT minimum value
IMT_{max}	IMT maximum value
$\text{IMT}_{\text{median}}$	IMT median value
k	Coefficient of variation for speckle filtering
λ	Wavelength of ultrasound wave
λ_π	Lai and Chin snake energy regularization parameter, $E_{\text{snake}}(v)$
$\lambda_d \in \Re^+$	Rate of diffusion for the anisotropic diffusion filter
m_{i1} and m_{i2}	Mean values of two classes (asymptomatic and symptomatic, respectively)

m/s and cm/s	Meters per second and centimeters per second, respectively
μ	Mean
N	Number of scatterers within a resolution cell
N_{feat}	Number of features in the feature set
$n_{i,j}$	Multiplicative noise component (independent of $g_{i,j}$, with mean 0) on pixel i, j
$nl_{i,j}$	Multiplicative noise component after logarithmic compression on pixel i, j
$n(s)$	Normal force tensor
ξ_i	Amount of ultrasound signal backscattered by scatterer i
$p_x(i)$	ith entry in the marginal probability matrix obtained by summing the rows of $p(i, j)$
Q	Mathematically defined universal quality index
$R = 1 - \frac{1}{1+\sigma^2}$	Smoothness of an image
Score_Dis	Score distance between two classes (asymptomatic, symptomatic)
$s_e = \sigma_{IMT}/\sqrt{2}$	Inter-observer error
$s_{\max}$	Maximum pixel value in the image
s^2	Structural energy
σ_{IMT}	IMT standard deviation
σ_{fg}	Covariance between two images f and g
σ	Standard deviation
σ^2	Variance
σ^3	Skewness
σ^4	Kurtosis
σ_{i1} and σ_{i2}	Standard deviations of two classes (asymptomatic and symptomatic, respectively)
$2\sigma^2$	Diffuse energy
σ_n	Standard deviation of the noise
$\}_{w}^2$	Variance of the gray values in a pixel window

List of Abbreviations

ACSRS	Asymptomatic carotid stenosis
DsFad	Perona and Malik anisotropic diffusion filter
DsFadsr	Speckle reducing anisotropic diffusion filter
ASM	Angular second moment
ATL HDI-3000	ATL 3000 ultrasound scanner
ATL HDI-5000	ATL 5000 ultrasound scanner
DsFca	Linear scaling of the gray-level despeckle filter
CAT	Computer-assisted tomography
CCA	Common carotid artery
CSR	Contrast-to-speckle radio
CT	Computer tomography
CW	Continuous wave
DR	Dynamic range
DS	Despeckled
DSCQS	Double stimulus continuous quality scale
DSIS	Double stimulus impairment scale
DVD	Digital video
DWT	Discrete wavelet transform
E	Effectiveness measure
ECA	External carotid artery
ECST	European carotid surgery trial
DsQEErr	Error summation in the form of the Minkowski metric
FDTA	Fractal dimension texture analysis
FFT	Fast Fourier transform
FPS	Fourier power spectrum
GAE	Geometric average error
GF	Geometric filtering
DsFgf4d	Geometric despeckle filter
DsFgfminmax	Geometric despeckle filter utilizing minimum maximum values
GGVF	Generalized gradient vector flow

GLDS	Gray-level difference statistics
GVF	Gradient vector flow
HD	Hausdorff distance
HF	Maximum homogeneity
HM	Homomorphic
DsFhomo	Homomorphic despeckle filter
DsFhomog	Most homogeneous neighbourhood despeckle filter
HVS	Human visual system
ICA	Internal carotid artery
IDM	Inverse difference moment
IDV	Intensity difference vector
IMC	Intima–media complex
IMT	Intima–media thickness
IVUS	Intravascular ultrasound
kNN	The statistical *k*-nearest-neighbor classifier
DsFlecasort	Linear scaling and sorting despeckle filter
LS	Linear scaling
DsFls	Linear scaling of the gray-level values despeckle filter
DsFlsmedcd	Lee diffusion despeckle filter
DsFlsminsc	Minimum speckle index homogeneous mask despeckle filter
DsFlsminv1d	Minimum variance homogeneous 1D mask despeckle filter
DsFlsmv	Mean and variance local statistics despeckle filter
DsFlsmvsk2d	Mean variance, higher moments local statistics despeckle filter
DsFlsmvske1d	Mean, variance, skewness, kurtosis 1D local statistics despeckle filter
M	Manual
DsFmedian	Median despeckle filter
MF	Multi-resolution fractal
MMSE	Minimum mean-square error
MN	Manual normalized
MRI	Magnetic resonance imaging
MSE	Mean square error
N	Normalized
ND	Normalized despeckled
NE	North–east
NF	No filtering

NGTDM	Neighborhood gray-tone difference matrix
NIE	Normalized image energy
DsFnldif	Nonlinear coherent diffusion despeckle filter
NS	Not significant difference
NST	North–south
NTSE	Normalized total snake energy
P	Precision
PDE	Partial differential equation
PDF	Probability density function
PET	Positron emission tomography
DsQEPSNR	Peak signal-to-noise radio
PW	Pulsed wave
R	Sensitivity (or recall)
RF	Radio frequency
DsQERMSE	Root mean square error
ROC	Receiver operating characteristic
S	Significant difference
Sp	Specificity
SAR	Synthetic aperture radar
SD	Standard deviation
SE	South–east
SFM	Statistical feature matrix
SGLDM	Spatial gray-level dependence matrices
SGLDMm	Spatial gray-level dependence matrix mean values
SGLDMr	Spatial gray-level dependence matrix range of values
DsQESNR	Signal-to-noise radio
SPECT	Single photon emission computer tomography
SSIN	Structural similarity index
TEM	Laws texture energy measures
TGC	Time gain compensation
TIA	Transient ischemic attacks
TV	Television
DsFwaveltc	Wavelet despeckle filter
WE	West–east
wiener	Wiener despeckle filter

WN	West–north
WS	West–south
WT	Wavelet transform
β_{err}	Minkowski error coefficient
1D	One-dimensional
2D	Two-dimensional
3D	Three-dimensional

References

[1] D. Lamont, L. Parker, M. White, N. Unwin, S.M.A. Bennett, M. Cohen, D. Richardson, H.O. Dickinson, A. Adamson, K.G.M.M. Alberti, A.W. Craft, "Risk of cardiovascular disease measured by carotid intima–media thickness at age 49–51: Life course study," *BMJ*, vol. 320, pp. 273–278, January 29, 2000, doi:10.1136/bmj.320.7230.273.

[2] C.B. Burckhardt, "Speckle in ultrasound B-mode scans," *IEEE Trans. Sonics Ultrasonics*, vol. SU-25, no. 1, pp. 1–6, 1978.

[3] R.F. Wagner, S.W. Smith, J.M. Sandrik, and H. Lopez, "Statistics of speckle in ultrasound B-scans," *IEEE Trans. Sonics Ultrasonics*, vol. 30, pp. 156–163, 1983.

[4] J.W. Goodman, "Some fundamental properties of speckle," *J. Opt. Soc. Am.*, vol. 66, no. 11, pp. 1145–1149, 1976.

[5] Y. Yongjian and S.T. Acton, "Speckle reducing anisotropic diffusion," *IEEE Trans. Image Process.*, vol. 11, no. 11, pp. 1260–1270, November 2002, doi:10.1109/TIP.2002.804276.

[6] R.W. Prager, A.H. Gee, G.M. Treece, and L. Berman, "Speckle detection in ultrasound images using first order statistics," *GUED/F-INFENG/TR 415*, University of Cambridge, Dept. of Engineering, pp. 1–17, July 2002.

[7] C.P. Loizou, C.S. Pattichis, C.I. Christodoulou, R.S.H. Istepanian, M. Pantziaris, and A. Nicolaides "Comparative evaluation of despeckle filtering in ultrasound imaging of the carotid artery," *IEEE Trans. Ultrason. Ferroelectr. Freq. Control*, vol. 52, no. 10, pp. 1653–1669, 2005.

[8] C.I. Christodoulou, C. Loizou, C.S. Pattichis, M. Pantziaris, E. Kyriakou, M.S. Pattichis, C.N. Schizas, and A. Nicolaides,"Despeckle filtering in ultrasound imaging of the carotid artery," in *Second Joint EMBS/BMES Conference, Houston, TX*, vol. 2, pp. 1027–1028, October 23–26, 2002.

[9] J.S. Lee, "Speckle analysis and smoothing of synthetic aperture radar images," *Comp. Graphics Image Process.*, vol. 17, pp. 24–32, 1981, doi:10.1016/S0146-664X(81)80005-6.

[10] L. Busse, T.R. Crimmins, and J.R. Fienup, "A model based approach to improve the performance of the geometric filtering speckle reduction algorithm," *IEEE Ultrasonic Symp.*, vol. 2, pp. 1353–1356, 1995, doi:10.1109/ULTSYM.1995.495807.

[11] D.T. Kuan, A.A. Sawchuk, T.C. Strand, and P. Chavel, "Adaptive restoration of images with speckle," *IEEE Trans. Acoust.*, vol. ASSP-35, pp. 373–383, 1987, doi:10.1109/TASSP.1987.1165131.

[12] M. Insana, T.J. Hall, G.C. Glendon, and S.J. Posental, "Progress in quantitative ultrasonic imaging," *SPIE Vol. 1090 Medical Imaging III, Image Formation*, pp. 2–9, 1989.

[13] V.S. Frost, J.A. Stiles, K.S. Shanmugan, and J.C. Holtzman, "A model for radar images and its application for adaptive digital filtering of multiplicative noise," *IEEE Trans. Pattern Anal. Mach. Intell.*, vol. 4, no. 2, pp. 157–165, 1982.

[14] J.S. Lee, "Digital image enhancement and noise filtering by using local statistics," *IEEE Trans. Pattern Anal. Mach. Intell.*, PAMI-2, no. 2, pp. 165–168, 1980.

[15] J.S. Lee, "Refined filtering of image noise using local statistics," *Comput. Graphics Image Process*, vol. 15, pp. 380–389, 1981.

[16] D.T. Kuan and A.A. Sawchuk, "Adaptive noise smoothing filter for images with signal dependent noise," *IEEE Trans. Pattern Anal. Mach. Intell.*, vol. PAMI-7, no. 2, pp. 165–177, 1985.

[17] S. Solbo and T. Eltoft, "Homomorphic wavelet based-statistical despeckling of SAR images," *IEEE Trans. Geosci. Remote Sens.*, vol. 42, no. 4, pp. 711–721, 2004.

[18] J. Saniie, T. Wang, and N. Bilgutay, "Analysis of homomorphic processing for ultrasonic grain signal characterization," *IEEE Trans. Ultrason. Ferroelectr. Freq. Control*, vol. 3, pp. 365–375, 1989, doi:10.1109/58.19177.

[19] S. Jin, Y. Wang, and J. Hiller, "An adaptive non-linear diffusion algorithm for filtering medical images," *IEEE Trans. Inf. Technol. Biomed.*, vol. 4, no. 4, pp. 298–305, December 2000.

[20] J. Weickert, B. Romery, and M. Viergever, "Efficient and reliable schemes for nonlinear diffusion filtering," *IEEE Trans. Image Process.*, vol. 7, pp. 398–410, 1998.

[21] N. Rougon and F. Preteux, "Controlled anisotropic diffusion," in *Conference on Nonlinear Image Processing VI, IS&T/SPIE Symposium on Electronic Imaging, Science and Technology, San Jose, CA*, pp. 1–12, February 5–10, 1995.

[22] M. Black, G. Sapiro, D. Marimont, and D. Heeger, "Robust anisotropic diffusion," *IEEE Trans. Image Process.*, vol. 7, no. 3, pp. 421–432, March 1998, doi:10.1109/83.661192.

[23] P. Rerona and J. Malik, "Scale-space and edge detection using anisotropic diffusion," *IEEE Trans. Pattern Anal. Mach. Intell.*, vol. 12, no. 7, pp. 629–639, July 1990.

[24] K. Abd-Elmoniem, A.-B. Youssef, and Y. Kadah, "Real-time speckle reduction and coherence enhancement in ultrasound imaging via nonlinear anisotropic diffusion," *IEEE Trans. Biomed. Eng.*, vol. 49, no. 9, pp. 997–1014, Sept. 2002, doi:10.1109/TBME.2002.1028423.

[25] S. Zhong and V. Cherkassky, "Image denoising using wavelet thresholding and model selection," in *Proceedings of the IEEE International Conference on Image Processing, Vancouver, BC, Canada*, pp. 1–4, November 2000.

[26] A. Achim, A. Bezerianos and P. Tsakalides, "Novel Bayesian multiscale method for speckle removal in medical ultrasound images," *IEEE Trans. Med. Imaging*, vol. 20, no. 8, pp. 772–783, 2001, doi:10.1109/42.938245.

[27] X. Zong, A. Laine, and E. Geiser, "Speckle reduction and contrast enhancement of echocardiograms via multiscale nonlinear processing," *IEEE Trans. Med. Imaging*, vol. 17, no. 4, pp. 532–540, 1998.

[28] X. Hao, S. Gao, and X. Gao, "A novel multiscale nonlinear thresholding method for ultrasonic speckle suppressing," *IEEE Trans. Med. Imaging*, vol. 18, no. 9, pp. 787–794, 1999.

[29] D.L. Donoho, "Denoising by soft thresholding," *IEEE Trans. Inform. Theory*, vol. 41, pp. 613–627, 1995.

[30] A.M. Wink and J.B.T.M. Roerdink, "Denoising functional MR images: A comparison of wavelet denoising and Gaussian smoothing," *IEEE Trans. Med. Imaging*, vol. 23, no. 3, pp. 374–387, 2004, doi:10.1109/TMI.2004.824234.

[31] V. Dutt, "Statistical analysis of ultrasound echo envelope," Ph.D. dissertation, Mayo Graduate School, Rochester, MN, 1995.

[32] M. Nagao and T. Matsuyama, "Edge preserving smoothing," *Computer Graphic and Image Processing*, vol. 9, pp. 394–407, 1979, doi:10.1016/0146-664X(79)90102-3.

[33] T. Huang, G. Yang, and G. Tang, "A fast two-dimensional median filtering algorithm," *IEEE Trans. Acoustics, Speech and Signal Processing*, vol. 27, no. 1, pp. 13–18, 1979, doi:10.1109/TASSP.1979.1163188.

[34] S.M. Ali and R.E. Burge, "New automatic techniques for smoothing and segmenting SAR images," *Signal Processing*, North-Holland, vol. 14, pp. 335–346, 1988, doi:10.1016/0165-1684(88)90092-8.

[35] F.N.S Medeiros, N.D.A. Mascarenhas, R.C.P Marques, and C.M. Laprano, "Edge preserving wavelet speckle filtering," in *5th IEEE Southwest Symposium on Image Analysis and Interpretation, Santa Fe, NM*, pp. 281–285, April 7–9, 2002, doi:10.1109/IAI.2002.999933.

[36] P. Moulin, "Multiscale image decomposition and wavelets," in *Handbook of Image & Video Processing*, A. Bovik (ed.), Academic Press, New York, pp. 289–300, 2000.

[37] P. Scheunders, "Wavelet thresholding of multivalued images," *IEEE Trans. Image Process.*, vol. 13, no. 4, pp. 475–483, 2004, doi:10.1109/TIP.2004.823829.

[38] S. Gupta, R.C. Chauhan, and S.C. Sexana, "Wavelet-based statistical approach for speckle reduction in medical ultrasound images," *Med. Biol. Eng. Comput.*, vol. 42, pp. 189–192, 2004, doi:10.1007/BF02344630.

[39] Philips Medical System Company, "Comparison of image clarity, SonoCT real-time compound imaging versus conventional 2D ultrasound imaging," *ATL Ultrasound Report*, 2001.

[40] C. Christodoulou, C. Pattichis, M. Pantziaris, and A. Nicolaides, "Texture-based classification of atherosclerotic carotid plaques," *IEEE Trans. Med. Imaging*, vol. 22, no. 7, pp. 902–912, 2003, doi:10.1109/TMI.2003.815066.

[41] R.M. Haralick, K. Shanmugam, and I. Dinstein, "Texture features for image classification," *IEEE Trans. Syst. Man Cybern.*, vol. SMC-3, pp. 610–621, November 1973.

[42] J.S Weszka., C.R. Dyer, and A. Rosenfield, "A comparative study of texture measures for terrain classification," *IEEE Trans. Syst. Man Cybern.*, vol. SMC-6, pp. 269–285, April 1976.

[43] M. Amadasun and R. King, "Textural features corresponding to textural properties," *IEEE Trans. Syst. Man Cybern.*, vol. 19, no. 5, pp. 1264–1274, Sept. 1989, doi:10.1109/21.44046.

[44] C.M. Wu, Y.C. Chen, and K.-S. Hsieh, "Texture features for classification of ultrasonic images," *IEEE Trans. Med. Imaging*, vol. 11, pp. 141–152, June 1992.

[45] T.J. Chen, K.S. Chuang, Jay Wu, S.C. Chen, I.M. Hwang, and M.L. Jan, "A novel image quality index using Moran I statistics," *Phys. Med. Biol.*, vol. 48, pp. 131–137, 2003.

[46] R. Gonzalez and R. Woods, *Digital image processing,* 2nd ed., Addison-Wesley Longman Publishing Co., Inc. Boston, MA, USA, 2002.

[47] Z. Wang, A. Bovik, H. Sheikh, and E. Simoncelli, "Image quality assessment: From error measurement to structural similarity," *IEEE Trans. Image Process.*, vol. 13, no. 4, pp. 600–612, April 2004, doi:10.1109/TIP.2003.819861.

[48] S. Winkler, "Vision models and quality metrics for image processing applications," PhD Dissertation, University of Lausanne, Lausanne, Switzerland, December 21, 2000.

[49] D. Sakrison, "On the role of observer and a distortion measure in image transmission," *IEEE Trans. Comm.,* vol. 25, pp. 1251–1267, November 1977, doi:10.1109/TCOM.1977.1093773.

[50] Z. Wang and A. Bovik, "A universal quality index," *IEEE Signal Process. Lett.*, vol. 9, no. 3, pp. 81–84, March 2002.

[51] H.R. Sheikh, A.C. Bovik, and G. de Veciana, "An information fidelity criterion for image quality assessment using natural scene statistics," *IEEE Trans. Image Process.*, vol. 14, no. 12, pp. 2117–2128, December 2005.

[52] E. Krupinski, H. Kundel, P. Judy, and C. Nodine, "The medical image perception society, key issues for image perception research," *Radiology*, vol. 209, pp. 611–612, 1998.

[53] T. Elatrozy, A. Nicolaides, T. Tegos, A. Zarka, M. Griffin, and M. Sabetai, "The effect of B-mode ultrasonic image standardization of the echodensity of symptomatic and asymptomatic carotid bifurcation plaque," *Int. Angiol.*, vol. 17, pp. 179–186, no. 3, Sept. 1998.

[54] C.P. Loizou, C.S. Pattichis, M. Pantziaris, T. Tyllis, and A. Nicolaides, "Snakes based segmentation of the common carotid artery intima media," *Med. Biol. Eng. Comput.*, vol.45, no. 1, pp. 35–49, January 2007.

[55] C.S. Pattichis, C. Christodoulou, E. Kyriakou, M. Pantziaris, A. Nicolaides, M.S. Pattichis, and C.P. Loizou, "Ultrasound imaging of carotid atherosclerosis," in *Wiley encyclo-*

paedia of biomedical engineering, M. Akay (ed.), Hoboken, NJ: John Wiley & Sons, Inc., 2006.

[56] J.C. Dainty, *Laser speckle and related phenomena*, Berlin: Springer-Verlag, 1974.

[57] J.U. Quistgaard, "Signal acquisition and processing in medical diagnostic ultrasound," *IEEE Signal Process. Mag.*, vol. 14, no. 1, pp. 67–74, January 1997, doi:10.1109/79.560325.

[58] H. Paul and H.P. Schwann, "Mechanism of absorption of ultrasound in liver tissue," *J Acoust. Soc. Am.*, vol. 50, pp. 692, 1971, doi:10.1121/1.1912685.

[59] C.P. Loizou, C.S. Pattichis, M. Pantziaris, T. Tyllis, and A. Nicolaides, "Quantitative quality evaluation of ultrasound imaging in the carotid artery," *Med. Biol. Eng. Comput.*, vol. 44, no. 5, pp. 414–426, 2006.

[60] C.P. Loizou, C.S. Pattichis, M. Pantziaris, and A. Nicolaides, "An integrated system for the segmentation of atherosclerotic carotid plaque," *IEEE Trans. Inform. Technol. Biomed.*, vol. 11, no. 5, pp. 661–667, November 2007.

[61] T. Greiner, C.P. Loizou, M. Pandit, J. Mauruschat, and F.W. Albert, "Speckle reduction in ultrasonic imaging for medical applications," *Proceedings of the ICASSP91, 1991 International Conference on Acoustic Signal Speech and Processing, Toronto, ON, Canada*, pp. 2993–2996, May 14–17, 1991, doi:10.1109/ICASSP.1991.151032.

[62] R.N. Czerwinski, D.L. Jones, and W.D. O'Brien, "Detection and boundaries in speckle images—Application to medical ultrasound," *IEEE Trans. Med. Imaging*, vol. 18, no. 2, pp. 126–136, February 1999, doi:10.1109/42.759114.

[63] M. Karaman, M. Alper Kutay, and G. Bozdagi, "An adaptive speckle suppression filter for medical ultrasonic imaging," *IEEE Trans. Med. Imaging,* vol. 14, no. 2, pp. 283–292, 1995.

[64] A.M. Wink and J.B.T.M. Roerdink, "Denoising functional MR images: A comparison of wavelet denoising and Gaussian smoothing," *IEEE Trans. Med. Imaging*, vol. 23, no. 3, pp. 374–387, 2004, doi:10.1109/TMI.2004.824234.

[65] S. Jin, Y. Wang, and J. Hiller, "An adaptive non-linear diffusion algorithm for filtering medical images," *IEEE Trans. Inform. Technol. Biomed.*, vol. 4, no. 4, pp. 298–305, December 2000.

[66] H.-L. Eng and K.-K. Ma, "Noise adaptive soft-switching median filter," *IEEE Trans. Image Process.*, vol. 10, no. 2, pp. 242–251, 2001.

[67] B. Fetics, E.Y. Wong, T. Murabarashi, G.S. Nelson, M.-M. Cohen, C.E. Rochitte, J.L. Weiss, D.A. Kass, E. Nevo, "Enhancement of contrast echocardiography by image variability analysis," *IEEE Trans. Med. Imaging*, vol. 20, no. 11, pp. 1123–1130, November 2001, doi:10.1109/42.963815.

[68] F. Rakebrandt, "Relation between ultrasound texture classification images and histology of atherosclerotic plaque," *Ultrasound Med. Biol.*, vol. 26, no. 9, pp. 1393–1402, 2000.

[69] M. Pattichis, C. Pattichis, M. Avraam, A. Bovik, and K. Kyriakou, "AM–FM texture segmentation in electron microscopic muscle imaging," *IEEE Trans. Med. Imaging*, vol. 19, no. 12, pp. 1253–1258, 2000, doi:10.1109/42.897818.

[70] N. Mudigonda, R. Rangayyan, and J. Desautels, "Detection of breast masses in mammograms by density slicing and texture flow-field analysis," *IEEE Trans. Med. Imaging*, vol. 20, no. 12, pp. 121–1227, December 2001, doi:10.1109/42.974917.

[71] C.I. Christodoulou, S.C. Michaelides, and C.S. Pattichis, "Multi-feature texture analysis for the classification of clouds in satellite imagery," *IEEE Trans. Geosci. Remote Sens.*, vol. 41, no. 11, pp. 2662–2668, November 2003.

[72] C.K. Zarins, C.Xu, and S. Glagov, "Atherosclerotic enlargement of the human abdominal aorta," *Atherosclerosis*, vol. 155, no. 1, pp. 157–164, 2001, doi:10.1016/S0021-9150(00)00527-X.

[73] N. Mudigonda, R. Rangayyan, and J. Desautels, "Detection of breast masses in mammograms by density slicing and texture flow-field analysis," *IEEE Trans. Med. Imaging*, vol. 20, no. 12, pp. 121–1227, December 2001.

[74] A. Pommert and K. Hoehne, "Evaluation of image quality in medical volume visualization: The state of the art," in *Medical image computing and computer-assisted intervention*, T. Dohi and R. Kikinis (eds.), *Proceedings of the MICCAI, 2002, Part II, Lecture Notes in Computer Science 2489*, Berlin: Springer-Verlag, pp. 598–605, 2002, doi:10.1007/3-540-45787-9_75.

[75] J.E. Wilhjelm, M.S. Jensen, S.K. Jespersen, B. Sahl, and E. Falk, "Visual and quantitative evaluation of selected image combination schemes in ultrasound spatial compound scanning," *IEEE Trans. Med. Imaging*, vol. 23, no. 2, pp. 181–190, 2004, doi:10.1109/TMI.2003.822824.

[76] M. Eckert, "Perceptual quality metrics applied to still image compression," in *Canon information systems research*, Faculty of Engineering, University of Technology, Sydney, Australia, pp. 1–26, 2002.

[77] A. Baraldi and F. Pannigianni, "A refined gamma MAP SAR speckle filter with improved geometrical adaptivity," *IEEE Trans. Geosci. Remote Sens.*, vol. 33, no. 5, pp. 1245–1257, September 1995, doi:10.1109/36.469489.

[78] E. Trouve, Y. Chambenoit, N. Classeau, and P. Bolon, "Statistical and operational performance assessment of multi-temporal SAR image filtering," *IEEE Trans. Geosc. Remote Sens.*, vol. 41, no. 11, pp. 2519–2539, 2003, doi:10.1109/TGRS.2003.817270.

[79] D. Schilling and P.C. Cosman, "Image quality evaluation based on recognition times for fast browsing image applications," *IEEE Trans. Multimedia*, vol. 4, no. 3, pp. 320–331, Sept. 2002, doi:10.1109/TMM.2002.802844.

[80] B.B. Mandelbrot, *The fractal geometry of nature*, San Francisco, CA: Freeman, 1982.

[81] L.J. Porcello, N.G. Massey, R.B. Ines, and J.M. Marks, "Speckle reduction in synthetic aperture radar images," *J. Opt. Soc. Am.*, vol. 66, no. 11, pp. 1305–1311, November 1976.

[82] C.P. Loizou, C. Christodoulou, C.S. Pattichis, R. Istepanian, M. Pantziaris, and A. Nicolaides, "Speckle reduction in ultrasound images of atherosclerotic carotid plaque," in *DSP 2002, Proceedings of the IEEE 14th International Conference on Digital Signal Processing, Santorini, Greece*, pp. 525–528, July 1–3, 2002, doi:10.1109/ICDSP.2002.1028143.

[83] J.M. Thijssen, B.J. Oosterveld, P.C. Hartman, G.J. Rosenbusch, "Correlations between acoustic and texture parameters from RF and B-mode liver echograms," *Ultrasound Med. Biol.*, vol. 19, pp. 13–20, 1993.

[84] Imaging Department, Johns Hopkins Bayview Medical Center, Baltimore, MD, http://www.jhbmc.jhu.edu/Imaging/index.html.

[85] K.T. Dussik, "On the possibility of using ultrasound waves as a diagnostic aid," *Neurol. Psychiatr.*, vol. 174, pp. 153–168, 1942.

[86] A. Kurjak, "Ultrasound scanning—Prof. Ian Donald (1910–1987)," *Eur. J. Obstet. Gynecol. Reprod. Biol.*, vol. 90, no. 2, pp. 187–189, June 2000, doi:10.1016/S0301-2115(00)00270-0.

[87] S.-M. Wu, Y.-W. Shau, F.-C. Chong, and F.-J. Hsieh, "Non-invasive assessment of arterial dimension waveforms using gradient-based Hough transform and power Doppler ultrasound imaging," *J. Med. Biol. Eng. Comput.*, vol. 39, pp. 627–632, 2001, doi:10.1007/BF02345433.

[88] W.R. Hedrick and D.L. Hykes, "Image and signal processing in diagnostic ultrasound imaging," *Journal of Diagnostic Medical Sonography*, vol. 5, no. 5, pp. 231–239, 1989, doi:10.1177/875647938900500502.

[89] F.J. Polak, "Doppler sonography: An overview," in *Peripheral vascular sonography: A practical guide*, Baltimore, MD: Williams & Wilkins, pp. 155–160, 1992.

[90] A. Ahumada and C. Null, "Image quality: A multidimensional problem," in *Digital images and human vision*, A.B. Watson (ed.), Cambridge, MA: Bradford Press, pp. 141–148, 1993.

[91] G. Deffner, "Evaluation of display image quality: Experts vs. non-experts," *Symp. Soc. Inf. Display Dig.*, vol. 25, pp. 475–478, 1994.

[92] E.A. Fedorovskaya, H. De Ridder, and F.J. Blomaert, "Chroma variations and perceived quality of colour images and natural scenes," *Color Res. Appl.*, vol. 22, no. 2, pp. 96–110, 1997, doi:10.1002/(SICI)1520-6378(199704)22:2<96::AID-COL5>3.0.CO;2-Z.

[93] E. Kyriakou, M.S. Pattichis, C.I. Christodoulou, C.S. Pattichis, S. Kakkos, M. Griffin, and A.N. Nicolaides, "Ultrasound imaging in the analysis of carotid plaque morphology for the assessment of stroke," in *Plaque imaging: Pixel to molecular level*, J.S. Suri, C. Yuan, D.L. Wilson, and S. Laxminarayan (eds.), IOS Press, Amsterdam, pp. 241–275, 2005.

[94] A.N. Nicolaides, M. Sabetai, S.K. Kakkos, S. Dhanjil, T. Tegos, and J.M. Stevens, "The asymptomatic carotid stenosis and risk of stroke study," *Int. Angiol.*, vol. 22, no. 3, pp. 263–272, 2003.

[95] J.C. Bamber and C. Daft, "Adaptive filtering for reduction of speckle in ultrasonic pulse-echo images," *Ultrasonic*, vol. 24, pp. 41–44, 1986, doi:10.1016/0041-624X(86)90072-7.

[96] J.T.M. Verhoeven and J.M. Thijssen, "Improvement of lesion detectability by speckle reduction filtering: A quantitative study," *Ultrasonic Imaging*, vol. 15, pp. 181–204, 1993, doi:10.1006/uimg.1993.1012.

[97] C. Kotropoulos and I. Pitas, "Optimum nonlinear signal detection and estimation in the presence of ultrasonic speckle," *Ultrasonic Imaging*, vol. 14, pp. 249–275, 1992, doi:10.1016/0161-7346(92)90066-5.

[98] E. Brusseau, C.L. De Korte, C.L., F. Mastick, J. Schaar, and A.F.W. Van der Steen, "Fully automatic luminal contour segmentation in intracoronary ultrasound imaging—A statistical approach," *IEEE Trans. Med. Imaging*, vol. 23, no. 5, pp. 554–566, 2004, doi:10.1109/TMI.2004.825602.

[99] M.R. Cardinal, J. Meunier, G. Soulez, E. Thérasse, and G. Cloutier, "Intravascular ultrasound image segmentation: A fast-marching method," *Proc. MICCAI, LNCS 2879*, pp. 432–439, 2003.

[100] M.E. Olszewski, A. Wahle, S.C. Vigmostad, and M. Sonka, "Multidimensional segmentation of coronary intravascular ultrasound images using knowledge-based methods," *Med. Imaging: Image Process. Proc. SPIE*, 5747, pp. 496–504, 2005, doi:10.1117/12.595850.

[101] T. Loupas, W.N. McDicken, and P.L. Allan, "An adaptive weighted median filter for speckle suppression in medical ultrasonic images," *IEEE Trans. Circuits Syst.*, vol. 36, pp. 129–135, 1989, doi:10.1109/31.16577.

[102] A. Zahalka and A. Fenster, "An automated segmentation method for three-dimensional carotid ultrasound images," *Phys. Med. Biol.*, vol. 46, pp. 1321–1342, 2001.

[103] A. Hamou and M. El.-Sakka, "A novel segmentation technique for carotid ultrasound images," *Int. Conf. Acoustic Speech Signal Process., ICASSP*, vol. 3, pp. III-521–III-524, 2004, doi:10.1109/ICASSP.2004.1326596.

[104] D.F. Specht, "Probabilistic neural networks," *INNS Neural Networks*, vol. 3, no. 1, pp. 109–118, 1990, doi:10.1016/0893-6080(90)90049-Q.

[105] D. Williams and M. Shah, "A fast algorithm for active contour and curvature estimation," *GVCIP: Imag. Und.*, vol. 55, no. 1, pp. 14–26, 1992, doi:10.1016/1049-9660(92)90003-L.

[106] L.D. Cohen, "On active contour models and balloons," *CVGIP:IU*, vol. 53, no. 2, pp. 211–218, 1991, doi:10.1016/1049-9660(91)90028-N.

[107] K.F. Lai and R.T. Chin, "Deformable contours-modeling and extraction," *IEEE Trans. PAMI*, vol. 17, no. 11, pp. 1084–1090, 1995, doi:10.1109/34.473235.

[108] C. Xu and . Prince, "Generalized Gradient vector flow external forces for active contours," *Signal Process.*, vol.71, pp. 131–139, 1998, doi:10.1016/S0165-1684(98)00140-6.

[109] J. Smilowitz, J. Balog, H. Keller, G. Olivera, L.A. Dewerd, and T.R. Mackie, "A new multipurpose quality assurance phantom for clinical tomotherapy," in *Proceedings of the 22nd Annual EMBS International Conference*, pp. 1191–1194, July 23–28, 2000, doi:10.1109/IEMBS.2000.897941.

[110] Loyola University Medical Center, Loyola University Chicago Stritch School of Medicine, Chicago, IL, http://www.meddean.luc.edu/lumen/MedEd/Neuro/index.htm.

[111] M.L. Bots, A.W. Hoes, P.J. Koudstaal, A. Hofman A, and D.E. Grobbee, "Common carotid intima-media thickness and risk of stroke and myocardial infarction: The Rotterdam Study," *Circulation*, vol. 96, pp. 1432–1437, 1997.

[112] J. E. Wilhjelm, M.L. Gronholdt, B. Wiebe, S.K. Jespersen, L.K. Hansen, and H. Sillesen, "Quantitative analysis of ultrasound B-mode images of carotid atherosclerotic plaque: Correlation with visual classification and histological examination," *IEEE Trans. Med Imaging*, vol. 17, no. 6, pp. 910–922, 1998, doi:10.1109/42.746624.

[113] D. Lamont, L. Parker, M. White, N. Unwin, S.M.A. Bennett, M. Cohen, D. Richardson, H.O. Dickinson, A. Adamson, K.G.M.M. Alberti, A.W. Craft, "Risk of cardiovascular disease measured by carotid intima–media thickness at age 49–51: Life course study," *BMJ*, vol. 320, pp. 273–278, 2000, doi:10.1136/bmj.320.7230.273.

[114] C.K. Zarins, C. Xu, and S. Glagov, "Atherosclerotic enlargement of the human abdominal aorta," *Atherosclerosis*, vol. 155, no. 1, pp. 157–164, 2001, doi:10.1016/S0021-9150(00)00527-X.

[115] ACAS Clinical Advisory, "Carotid endarterectomy for patients with asymptomatic internal carotid artery stenosis," *Stroke*, vol. 25, no. 12, pp. 2523–2524, 1994.

[116] Executive Committee for the Asymptomatic Carotid Atherosclerosis study, "Endarterectomy for asymptomatic carotid stenosis," *J. Am. Med. Assoc.*, vol. 273, pp. 1421–1428, 2002, doi:10.1109/79.774934.

[117] Y. Wang, J. Ostermann, and Y.-Q. Zhang, "Video processing and communications," in *Signal processing series*, A.V. Openheim (ser. ed.), Prentice-Hall, Upper Saddle River, New Jersey, USA, pp. 1–32, 2002.

[118] C. Stller and J. Konrad, "Estimating motion in image sequences," *IEEE Signal Process. Mag.*, vol. 16, pp. 70–91, July 1999.

[119] A. Kokaram, "Motion picture restoration," in *Digital algorithms for artefact suppression in degraded motion picture film and video*, London: Springer-Verlag, ch. 10, pp. 241–259, 1998.

[120] S. Winkler, "Digital video quality," in *Vision models and metrics*, John Wiley & Sons Ltd., England, pp. 71–102, 2005.

[121] M. Oezkan, A. Erdem, M. Sezan, and A. Tekalp, "Efficient multi-frame Wiener restoration of blurred and noisy image sequences," *IEEE Trans. Image Process.*, vol. 1, pp. 453–476, October 1992.

[122] P.M.B. Van Roosmalen, S.J.P Westen, R.L. Lagendijk, and J. Biemond, "Noise reduction for image sequences using an oriented pyramid threshold technique," *IEEE Int. Conf. Image Process.*, vol. 1, pp. 375–378, 1996, doi:10.1109/ICIP.1996.559511.

[123] M. Vetterli and J. Kovacevic, *Wavelets and subband coding*, Prentice-Hall, Signal Processing Series, Englewood Cliffs, NJ, 1995.

[124] J.-H. Jung, K. Hong, and S. Yang**,** "Noise reduction using variance characteristics in noisy image sequence," *Int. Conf. Consumer Electron.*, vol. 1, pp. 213–214, January 8–12, 2005.

[125] M. Bertalmio, V. Caselles, and A. Pardo, "Movie denoising by average of warped lines," *IEEE Trans. Image Process.***,** vol. 16, no. 9, pp. 233–2347, 2007, doi:10.1109/TIP.2007.901821.

[126] B. Alp, P. Haavisto, T. Jarske, K. Oestaemoe, and Y. Neuro, "Median based algorithms for image sequence processing," *SPIE Vis. Commun. Image Process.*, pp. 122–133, 1990, doi:10.1117/12.24175.

[127] J.T. Bushberg, J. Anthony Seibert, E.M. Leidholdt Jr., and J.M. Boone, *The essential physics of medical imaging*, Lippincott Williams & Wilkins, Philadelphia, USA 2002.

[128] I. Wendendelhag, Q. Liang, T. Gustavsson, and J. Wikstrand, "A new automated computerized analysing system simplifies reading and reduces the variability in ultrasound measurement of intima media thickness," *Stroke*, vol. 28, pp. 2195–2200, 1997.

[129] V. Zlokolica, Advanced nonlinear methods for video denoising, Ph.D. dissertation, Ghent University, Belgium, 2006.

Author Biography

Christos P. Loizou was born in Cyprus on October 23, 1962, and received his BSc degree in electrical engineering and Dipl-Ing (MSc) degree in computer science and telecommunications from the University of Kaiserslautern, Kaiserslautern, Germany and his PhD degree on ultrasound image processing of the carotid artery from the Department of Computer Science, Kingston University, UK, in 1986, 1990, and 2005, respectively. He is an assistant professor at the Department of Computer Science, School of Sciences, Intercollege, Limassol, Cyprus, since 2000. He is also a research scientist at the Department of Computational Intelligence of the Cyprus Institute of Neurology and Genetics since 2001. From 1996 to 2000, he was a lecturer in the Department of Computer Science, Higher Technical Institute, Nicosia, Cyprus. He has been involved in numerous projects in these areas funded by the Cyprus Institute Promotion and Foundation, such as the IASIS, TALOS, NEVRORAFI, OPTOPOIISI, and Visema, with a total funding managed close to 1 million euros. He has published 5 chapters in books, 5 refereed journal articles, and 20 conference proceeding papers in these areas. His current research interests include medical imaging, signal and image processing, pattern recognition, biosignal analysis, and computer applications in medicine. He was a conference session chair of the *IEEE Information Technology in Biomedicine*, ITAB06. Dr. Loizou is a member of the IEEE and a senior member of the Institution of Electrical Engineers. He lives in Limassol, Cyprus, with his wife and children, a boy and a girl.

Constantinos S. Pattichis (S'88–M'88–SM'99) was born in Cyprus on January 30, 1959 and received his diploma as technician engineer from the Higher Technical Institute in Cyprus in 1979, his BSc in electrical engineering from the University of New Brunswick, Canada, in 1983, his MSc in biomedical engineering from the University of Texas at Austin, USA, in 1984, his MSc in neurology from the University of Newcastle Upon Tyne, UK, in 1991, and his PhD in electronic engineering from the University of London, UK, in 1992. He is currently a professor at the Department of Computer Science of the University of Cyprus. His research interests include ehealth, medical imaging, biosignal analysis, and intelligent systems. He has been involved in numerous projects in these areas funded by the EU, the National Research Foundation of Cyprus, the INTERREG, and other bodies, such as the IntraMEDNET, InterMed, Future Health, Ambulance, Emergency,

ACSRS, Telegyn, HealthNet, IASIS, Ippokratis, and others, with a total funding managed close to 5 million euros. He has published 47 refereed journal articles, 110 conference papers, and 17 chapters in books in these areas. He is coeditor of the books *M-Health: Emerging Mobile Health Systems*, published in 2006 by Springer, and *Information Technology in Biomedicine*, to be published in 2009 by IEEE. He was guest coeditor of the special issues on *Emerging Health Telematics Applications in Europe* and the forthcoming *Emerging Technologies in Biomedicine* and *Computational Intelligence in Medical Systems* of the *IEEE Transactions on Information Technology in Biomedicine*. He was general cochairman of the *Medical and Biological Engineering and Computing Conference* (MEDICON'98) and the IEEE Region 8 *Mediterranean Conference on Information Technology and Electrotechnology* (MELECON'2000) and program cochair of the *IEEE Information Technology in Biomedicine*, ITAB06. In addition, he served as an associate editor of the *IEEE Transactions on Information Technology in Biomedicine* and *IEEE Transactions on Neural Networks*. He served as chairperson of the Cyprus Association of Medical Physics and Biomedical Engineering (1996–1998) and the IEEE Cyprus Section (1998–2000). He is a senior member of IEEE.